博士論文

Studies on CT Diagnostic Imaging for the Hepatic and Pancreatic Disorders in Dogs

（犬における肝疾患および膵疾患の
CT 画像検査に関する研究）

Kenjiro Fukushima

福島　建次郎

Contents

General Introduction

There are several imaging modalities available in human and small animal practice including radiography, ultrasonography (US), computed tomography (CT) and magnetic resonance imaging. Among them, CT is widely applied in human medicine because it allows obtaining comprehensive and objective images in a relatively short time. Recently, along with the development of multi-detector row CT, high-speed and high-resolution imaging has become possible. Since high-speed imaging enabling multi-phasic contrast enhanced CT, it is possible to apply CT to precise evaluation of blood vessels and differential diagnosis of certain diseases.

Primary hepatic and pancreatic diseases are relatively common in veterinary clinical practice. There are several examinations to detect or diagnose hepatic and pancreatic diseases. While blood examination is useful for detecting or diagnosing some of the hepatic and pancreatic diseases, further imaging diagnosis is essential for definitive diagnosis or treatment planning in some of these diseases. For example, congenital portosystemic

shunt (cPSS) is one of the diseases of such kind. As cPSS is a disease of abnormal vessel originates from the portal system and connects to the systemic circulation, causing neurological, urological and systemic disorders. Although elevated fasting serum ammonia concentration and/or post-prandial serum bile acid concentration are reported to be useful for the detection of cPSS in dogs (Gerritzen-Bruning *et al.*, 2006), visualization of abnormal shunt vessel is needed for definitive diagnosis. It has been reported that ultrasonography (US) is one of the useful imaging modality to detect abnormal blood vessels in cPSS dogs (d'Anjou, 2004). Computed tomography (CT) is another imaging modality that is more useful for definitive diagnosis of cPSS than US in dogs. CT portography allows evaluating the morphological features of the shunt vessels in detail and classifying the anatomical shunt types (Nelson et al., 2011). Since cPSS can be cured by surgical attenuation of the shunt vessels, accurate understanding of the shunt vessels prior to surgery is important part of the diagnosis and treatment. In Chapter 1, in order to obtain information that is

useful for improving diagnostic accuracy of the extrahepatic congenital portosystemic shunt (EH-cPSS), I classified the EH-cPSS based on CT portographic findngs and clarified the clinical features of each shunt type.

Imaging diagnosis is also important for the diagnosis of hepatic mass forming diseases. It is known that US is quite useful screening examination to detect hepatic mass lesions. However, since information obtained by CT including size, number, location, vascular distribution of the tumor and presence or absence of metastasis, it is useful not only for detection but for staging and surgical planning superior to US. Actually in human medicine, CT is recommended in the patients with hepatic mass lesions for diagnosis and staging of the tumor (Choi *et al.*, 2014). Additionally, characteristic multiphasic CT findings of each hepatic mass lesion have been well described: e.g. hyper-attenuation in the arterial phase and hypo-attenuation in the venous phase were common findings in the progressed hepatocellular carcinoma. There are a lot of literatures regarding CT findings of hepatic mass lesions in human medicine, and relevant

systematic reviews described that the sensitivity of multi-phasic CT to diagnose hepatocellular carcinoma was 68 to 91% (Choi *et al.*, 2014; Lee *et al.*, 2015). However in the veterinary medicine, information about multi-phasic CT in the patients with hepatic mass lesions is quite limited. Therefore, in Chapter 2, image features of triple-phase CT to differentiate hepatic mass lesions were evaluated.

The pancreas is the largest gland in the digestive system and has both exocrine and endocrine functions. Although some exocrine and endocrine pancreatic disorders can be detected by blood examination (e.g. pancreatitis, pancreatic insulinoma), imaging is the important part of diagnosis and treatment planning. The pancreas is located in the cranial abdomen. The right lobe lies inside to dorsal to the descending duodenum and the left lobe lies dorsocaudal to the stomach and transverse colon. Although US is an useful imaging modality, the utility of US to evaluate the pancreas depends on each operator's skill, capability of the US equipment and interference from gastrointestinal contents (Penninck, 2013). In contrast,

CT is a useful modality to obtain the entire and objective images of the pancreas. Therefore, it is recommended to perform CT examination for the patients with pancreatic tumors in human medicine (Furlow, 2015). There is a review in which characteristic CT findings of pancreatic tumors were well described in humans (de la Santa t *et al.*, 2014). In that review, while the primary lesions of pancreatic adenocarcinoma showed hypo-attenuation at arterial phase, the metastatic lesions in the liver showed hypo-attenuation at portal phase in dual-phase CT. In contrast, it is common that the lesions with pancreatic insulinoma present hyper-attenuation in the arterial phase (Gouya *et al.*, 2003; Liu *et al.*, 2009). As described above, since CT findings of pancreatic tumors are well documented in humans, these findings are conceivably helpful to make a diagnosis of pancreatic tumors in dogs. In chapter 3, I evaluated image features of triple-phase CT to detect the canine pancreatic insulinomas.

Although CT is indispensable for the diagnosis and treatment planning of the diseases described above, information and evidence of their

CT findings are quite limited in small animal medicine. Therefore, each study in this thesis is focused on to clarify clinical features and characteristic CT findings of these diseases consequently improving the diagnostic accuracy, facilitating treatment choice and developing novel diagnostic methods of these diseases.

.

Chapter 1

Computed tomographic morphology and clinical features of extrahepatic portosystemic shunts in 172 dogs in Japan

Abstract

Canine extrahepatic congenital portosystemic shunts (EH-cPSS) are classified into several anatomic types, depending on their origin and termination of the shunt vessel. The aim of this chapter was to determine the proportion and clinical features of each anatomical shunt type in a population of dogs presented to the Veterinary Medical Center at the University of Tokyo. Dogs diagnosed with EH-cPSS using CT portography were included (n = 172) and shunts were classified based on previous reports. Clinical data were collected from case records and analyzed statistically. The most common anatomical type was the spleno-phrenic shunt (n = 64), followed by the spleno-azygos (n = 38), right gastric-caval (n = 29), spleno-caval (n = 21), right gastric-caval with caudal loop (n = 9), right gastric-phrenic (n = 6), colono-caval (n = 3), spleno-phrenic and azygos (n = 1), and porto-caval shunts (n = 1). Spleno-phrenic and spleno-azygos shunts were diagnosed significantly more frequently in older dogs than right gastric-caval and spleno-caval shunts ($P < 0.05$). The portal vein/aortic

(PV/Ao) ratio was significantly larger in dogs with spleno-phrenic shunt than in dogs with the spleno-azygos, right gastric-caval or spleno-caval shunts ($P < 0.05$). The PV/Ao ratio was significantly larger in dogs with spleno-azygos shunts than in dogs with right gastric-caval shunts. Dogs with spleno-phrenic shunts had significantly lower serum alkaline phosphatase activities than those with right gastric-caval or spleno-caval shunts. Dogs with spleno-phrenic shunts had significantly lower fasting ammonia concentrations than those with spleno-caval shunts. Since several clinical features evaluated in this chapter were significantly different depending on shunt types, thorough evaluation of shunt morphology by using CT portography is essential for the diagnosis of EH-cPSS in dogs.

Introduction

The prevalence of the congenital portosystemic shunt (cPSS) in dogs is reported to be 0.06-0.2% (Center, 1996). Extrahepatic congenital portosystemic shunts (EH-cPSS) are commonly diagnosed in young, purebred, and small breed dogs such as Yorkshire terriers, Maltese, Miniature schnauzers, and Cairn terriers. EH-cPSS are classified anatomically by their origin and termination. The four major shunt types are the spleno-caval, spleno-azygos, right gastric-caval, and right gastric-azygos shunts. Although some other types of shunt have also been reported, these are quite rare (Szatmari *et al.*, 2006).

Intraoperative mesenteric portography was formerly the most common method for the definitive diagnosis of EH-cPSS (Martin, 1993). Less invasive methods, such as ultrasonography (US) and computed tomographic (CT) portography, are recently used more commonly (d'Anjou *et al.*, 2004; Zwingenberger *et al.*, 2005). In particular, CT portography is useful for preoperative diagnosis and surgical planning, reducing the morbidity and

time associated with surgery (Frank *et al.*, 2003). More recently, the anatomical classification of the EH-cPSS in CT portography has been reported in detail and several novel types have been reported, including the spleno-phrenic shunt (Nelson *et al.*, 2011). Spleno-phrenic shunts have a characteristic termination of the shunt vessel, which drains into the caudal vena cava (CVC) cranial to the liver.

Since the relationship between different anatomical types of EH-cPSS and their clinical features has not been fully evaluated, the purpose of the study in this chapter was to clarify the proportion and clinical characteristics of each anatomical shunt type.

Materials and methods

Medical records from dogs diagnosed with EH-cPSS using CT portography at the Veterinary Medical Center at the University of Tokyo (VMC-UTokyo) from April 2007 to November 2012 were included in this study. Clinical data collected included breed, age, sex, body weight, and clinical signs related to the cPSS (seizure, depression, salivation, vomiting, and blindness) at first presentation to VMC-UTokyo. The results of blood test such as fasting ammonia (NH_3), pre- and post-prandial serum bile acid (SBA), blood urea nitrogen, serum glucose, serum albumin, alanine aminotransferase, and alkaline phosphatase (ALP) were also collected. In the dogs that underwent surgery, the difference of portal vein pressure before and after temporary occlusion of the shunt vessel, and the presence or absence of postoperative complications (post-ligation seizure, ascites, and gastrointestinal congestion) within 3 weeks were recorded.

Image analysis

All images were carefully reviewed on Osiri X (Pixmeo, Geneva,

Switzerland). Anatomical shunt types were classified based on the previous report (Nelson *et al.*, 2011) and novel classifications were made as necessary. The portal vein diameter was measured on transverse images halfway between the entrance of the gastroduodenal vein and the right portal branch to the liver. The aortic diameter was measured on the same transverse images. The portal vein/aortic (PV/Ao) ratio was calculated using these values (Nelson *et al.*, 2011). If the portal vein was undetectable at the previously noted location, the PV/Ao ratio was considered to be zero. The presence or absence of uroliths was also noted.

Statistical analysis

To evaluate the predisposition of EH-cPSS in each breed, all cases presented to VMC-UTokyo during the study period were used as the reference population. The odds ratio and 95% confidence interval (95% CI) were calculated if the number of cases was >5 in each breed category. If the lower limit of the 95% CI was >1, this considered to represent a significantly higher risk of EH-cPSS in the breed ($P < 0.05$).

To compare the clinical data for each morphologic classification, the Kruskall-Wallis test was used for statistical analysis and post-hoc comparison were performed using Dunn's multiple comparison tests. *P* values < 0.05 were considered to be significant. Groups of >10 cases for each anatomic shunt type were evaluated statistically.

Results

Medical record from 172 dogs were analyzed, consisting of 79 males (29 castrated) and 93 females (34 spayed). The median age and body weight were 22 months (range, 2–116 months) and 3.1 kg (range, 1–11.1 kg), respectively. Affected breeds and odds ratios are summarized in Table 1-1. Yorkshire terrier, Toy Poodle, Papillon, Miniature schnauzer and Norfolk terrier were at higher risk of having EH-cPSS ($P < 0.05$).

The most common anatomical type was the spleno-phrenic shunt (n = 64) followed by spleno-azygos (n = 38), right gastric-caval (n = 29), spleno-caval (n = 21), right gastric-caval with caudal loop (n = 9), right gastric-phrenic (n = 6), colono-caval (n = 3), spleno-phrenic and azygos (n = 1), and porto-caval shunts (n = 1). Individual breed numbers for each of the major 4 shunt types (spleno-phrenic, spleno-azygos, right gastric-caval, and spleno-caval shunts) are shown in Table 1-2 and their clinical features are summarized in Table 1-3. Volume rendering color images of representative examples of each of the four most prevalent shunt types are shown in Figure

1-1. Statistical analysis revealed a significant difference in age, PV/Ao ratio, fasting ammonia concentrations, and ALP activities among the shunt types ($P < 0.05$).

Spleno-phrenic shunts were diagnosed at a significantly older age than right gastric-caval and spleno-caval shunts ($P < 0.001$). Spleno-azygos shunts were diagnosed at a significantly older age than right gastric-caval and spleno-caval shunts ($P < 0.05$, $P < 0.01$, respectively; Figure 1-2).

PV/Ao ratios were significantly larger for spleno-phrenic shunt (median, 0.83) than spleno-azygos (median, 0.62; $P < 0.01$), right gastric-caval (median, 0.55; $P < 0.001$), and spleno-caval shunts (median, 0.55; $P < 0.001$). Spleno-azygos shunts were associated with significantly larger PV/Ao ratios than right gastric-caval shunt ($P < 0.05$; Figure 1-3). Patients with spleno-phrenic shunts had significantly lower serum ALP activities than those with right gastric-caval and spleno-caval shunts ($P < 0.01$; Figure 1-4). Patients with spleno-phrenic shunt had significantly lower fasting ammonia concentrations than those with spleno-caval shunt ($P <$

0.01; Figure 1-5). There were no significant differences in any other parameters evaluated in this study.

Clinical data for dogs with other types of shunts that were each represented at least three times in the study populations are shown in Table 1-3. Since the number of dogs with each of these shunt types was small, statistical analysis was not performed in these cases. Volume rendering images of these three shunt types are described in Figure 1-6.

Discussion

Spleno-phrenic shunts were the most common type of EH-cPSS in this population of dogs in Japan (37.2%). This is different from a previous report from North America, in which spleno-azygos shunts were the most common (32%), followed by spleno-caval (24%) and spleno-phrenic shunts (16%) (Nelson *et al.*, 2011). Since Miniature dachshunds and Toy poodles are popular in Japan and had relatively high prevalence of spleno-phrenic shunts (Table 7), geographical breed distribution or genetic bias may be responsible for this discrepancy.

Spleno-phrenic shunts were diagnosed at a significantly older age than right gastric-caval and spleno-caval shunts. Additionally, spleno-phrenic shunt presented with significantly larger PV/Ao ratios than the other shunt types. The phrenic vein drains into the CVC caudal to the diaphragm and cranial to the liver, and easily collapses with each respiratory cycle. This could contribute to decreased shunt fraction and result in latent clinical signs and preserved size of portal vein. Unfortunately,

because no cases underwent scintigraphy, the exact shunt fraction of each case was unknown. It has been reported that dogs with PV/Ao ratios >0.8 did not have the EH-cPSS on US evaluation (D'anjou *et al.*, 2004). However, 38 out of 64 cases in this study with spleno-phrenic shunts had PV/Ao ratios >0.8. Although different imaging modalities (US and CT) were used in the two studies, this type of shunt might not be diagnosed by US screening based on determining the PV/Ao ratio. The World Small Animal Veterinary Association (WSAVA) has established standardized methodology for US diagnosis of portosystemic shunts (Szatmari *et al.*, 2006). This standardized method is based on the concept that the shunts with caval termination drain into the CVC at the same location, i.e., slightly cranial to where the celiac artery originates from the aorta. Since the spleno-phrenic shunt drains into the CVC cranial to the liver, the termination of this shunt type cannot be detected by using the WSAVA method.

In addition, while the shunt vessel of the spleno-phrenic shunt is situated at the left and dorsal part of the body, the WSAVA method for PSS

mainly consists of planes from the right side of the body. Therefore, spleno-phrenic is potentially difficult to detect and it might not be visualized using these standardized planes. Since the spleno-phrenic shunt was relatively common in Japan, other diagnostic workup should be considered by analyzing the results obtained in this study.

Spleno-azygos shunts were diagnosed in significantly older dogs than right gastric-caval and spleno-caval shunts. This result corresponded to a previous report (Van den Bossche *et al.*, 2012), but the present study was able to describe the shunt morphology in more detail. Furthermore, spleno-azygos shunts had a significantly larger PV/Ao ratios than right gastric-caval shunts. In normal dogs, the diameter of the azygos vein is smaller than that of the CVC. Therefore, resistance to blood flow might be higher in azygos shunts than in caval shunts when the shunt vessels drain into the systemic circulation. This could result in relatively sustained PV diameter in spleno-azygos shunt compared to those in caval shunt, which have lower blood flow resistance. Additionally, most spleno-azygos shunts

have distinctly tortuous morphology, which could contribute to reduced blood flow. Furthermore, since azygos shunts penetrate the dorsal diaphragm and drain into the thorax, increased intrathoracic pressure or respiratory movement may also result in reduced blood flow. These mechanisms are likely similar to that of the spleno-phrenic shunts.

Serum ALP activities in dogs with spleno-phrenic shunts were significantly lower than those with right gastric-caval and spleno-caval shunts. Serum ALP activity (mainly bone-derived ALP) is highest during the first 16 weeks of life and then continued to decrease until 1 year of age (Fernandez *et al*, 2007). Since the age at diagnosis was significantly older in the spleno-phrenic shunt (median, 51.5 months) than in the right gastric-caval (median, 10.5 months) and spleno-phrenic shunts (median, 6 months), age might be responsible for these differences in serum ALP activities.

Fasting serum NH_3 concentrations were significantly lower in dogs with spleno-phrenic shunts (median, 87.5 μg/dL) than in those with

spleno-caval shunts (median, 171 μg/dL). In a previous report, there were no cPSS case among 132 dogs with fasting serum NH_3 < 78 μg/dL (Gerritzen-Bruning, 2006). In the study of this chapter, 26 out of 64 spleno-phrenic shunt cases presented with serum fasting NH_3 concentrations < 78 μg/dL. Reduced blood flow associated with the anatomical morphology of the shunt vessel may explain this difference. Regardless of shunt type, post-prandial SBA concentrations were elevated in most of the cases with EH-cPSS (99.3%) in the present study. Post-prandial SBA was the most sensitive biochemical screening test for the EH-cPSS.

This study revealed that Yorkshire terriers, Toy poodles, Papillons, Miniature schnauzers, and Norfolk terriers were at a significantly higher risk for the EH-cPSS in this Japanese population. These results are similar to previous reports from the Netherlands and North America (Van den Bossche *et al.*, 2012; Nelson *et al.*, 2011), with the exception of the high prevalence of EH-cPSS in Toy poodles in Japan. Toy poodles have became popular in Japan over the last decade and inbreeding might have resulted in

an increased risk of inherited conditions. A recent report showed no difference in breed distributions for porto-caval and porto-azygos shunts (Van den Bossche *et al.*, 2012), although anatomical shunt types were not classified in detail. Further investigation is needed to clarify potential breed predispositions to EH-cPSS and veterinarians must make effort to avoid inappropriate breeding.

In conclusion, spleno-phrenic shunts were the most common type of canine EH-cPSS in this study and there were significant clinical differences among anatomical shunt types, including age at presentation, PV/Ao ratio, serum ALP activity, and fasting serum NH_3 concentration. It is important to determine EH-cPSS morphology in detail and to understand that certain types of EH-cPSS could be difficult to detect using current diagnostic methods.

Table 1-1

Number of dogs of different breeds and odds ratios for extrahepatic congenital portosystemic shunts

Breed	*n*	Odds ratio (95% CI) [a]
Yorkshire terrier	28	4.10* (2.75–6.12)
Miniature dachshund	25	0.91 (0.60–1.39)
Toy poodle	18	1.85* (1.14–3.00)
Shih Tzu	16	1.66 (0.99–2.77)
Papillon	14	3.34* (1.94–5.73)
Miniature schnauzer	11	2.55* (1.39–4.68)
Chihuahua	11	0.90 (0.49–1.65)
Maltese	9	1.73 (0.89–3.38)
Norfolk terrier	8	24.00* (12.4–46.2)
Pug	5	1.89 (0.78–4.57)
Pomeranian	4	ND [b]
West Highland white terrier	3	ND [b]
Others [d]	20	ND [b]

[a] 95% CI, 95% confidence interval

[b] ND, not determined

[c] Breeds with a significantly higher risk of extrahepatic congenital portosystemic shunt

[d] Pembroke Welsh Corgi, Shetland sheepdog, Italian greyhound (*n* = 2 for each breed)

Shiba, Miniature pinscher, Bolognese, Jack Russell terrier, Cairn terrier (*n* = 1 for each breed)

Crossbred (*n* = 9)

* Breeds with significantly higher risk of EX-cPSS

Table 1-2

Number of dogs of different breeds with each shunt type

	Spleno-phrenic	Spleno-azygos	RG [a]-caval	Spleno-caval
Yorkshire terrier	5	6	7	5
Miniature dachshund	12	3	3	2
Toy poodle	8	8	0	1
Shih Tzu	6	4	2	1
Papillon	6	3	1	0
Miniature schnauzer	8	1	0	1
Chihuahua	7	0	3	0
Maltese	0	1	5	2
Norfolk terrier	1	4	2	1
Pug	2	1	1	0
Others	9	7	5	8
Total	64	38	29	21

[a] RG, right gastric

Table 1-3. Clinical features of the four major shunt types

	Spleno-phrenic (n = 64)	Spleno-azygos (n = 38)	RG[a]-caval (n = 29)	Spleno-caval (n = 21)
Age (months)	51.5 [1] (4–128)	33.5 [2, 3] (3–86)	10.5 [1, 3] (3–95)	6 [1, 2] (2–81)
Clinical signs (n)	27/61	17/37	14/26	10/20
Fasting NH_3 (mcg/dL)	87.5 [2] (24–748)	104 (46–393)	135 (53–490)	171 [2] (53–354)
Pre-prandial SBA[b] (nmol/L)	105.1 (5.8–400.0)	89.4 (19–543.3)	137.2 (15.1–539.7)	87.7 (13.9–437.8)
Post-prandial SBA[b] (nmol/L)	224.5 (21.7–502.5)	226.3 (49.0–432.8)	239.5 (78.3–613.7)	250.0 (126.9–490.0)
BUN[c] (mg/dL)	6.5 (2.1–23.9)	5.9 (2.4–13.3)	6.3 (1.6–12.6)	6.4 (1.1–12.6)
Glucose (mg/dL)	89.5 (44–131)	92 (28–137)	91.5 (59–125)	83 (48–127)
Albumin (g/dL)	2.9 (1.2–3.4)	2.8 (1.8–3.8)	2.6 (1.5–3.4)	2.7 (1.2–3.2)
ALT[d] (U/L)	84 (22–595)	95.5 (28–1,985)	108 (51–805)	103.5 (30–1,391)
ALP[e] (U/L)	197 [2] (61–2,600)	263.5 (116–1,674)	462.5 [2] (142–1,924)	546.5 [2] (99–2,165)
PV/Ao[f] ratio	0.83[1, 2] (0.37–1.31)	0.62 [2, 3] (0–1.30)	0.55[1, 3] (0–0.75)	0.55[1] (0–1.03)
Presence of urolith (n)	23/64	23/38	16/29	13/21
Received surgery (n)	30/53 (56.6%)	27/34 (79.4%)	21/25 (84.0%)	16/19 (84.2%)
PVP[g] difference (mmHg)	5 (0–33)	6 (1–42)	9 (0–19)	5.5 (1–37)
Post-surgical complications (n)	1/30	1/27	3/21	2/16

[1] $P < 0.001$, [2] $P < 0.01$, [3] $P < 0.05$

[a] RG, right gastric, [b] SBA, serum bile acid, [c] BUN, blood urea nitrogen, [d] ALT, alanine aminotransferase, [e] ALP, alkaline phosphatase, [f] PV/Ao, portal vein/aorta, [g] PVP, portal venous pressure, Median (range) shown when applicable.

Table1-4 Clinical features of the minor shunt types

	RG[a]-caval Ca loop (n = 9)	RG[a]-phrenic (n = 6)	Colono-caval (n = 3)
Age (months)	44.0 (7–98)	16.0 (12–68)	65.0 (13–92)
Clinical signs (n)	5/9	1/5	2/3
Fasting NH_3 (mcg/dL)	217 (62–515)	114 (86–256)	62 (53–72)
Pre-prandial SBA[b] (nmol/L)	157.0 (58.9–348.6)	122.8 (24.6–271.9)	213.7 (59.4–372)
Post-prandial SBA[b] (nmol/L)	237.2 (34.8–329.7)	248.3 (177.8–281.4)	251.8 (250.0–253.5)
BUN[c] (mg/dL)	7.9 (3.6–13.5)	8.4 (3.7–15.3)	6.1 (5.3–12.8)
Glucose (mg/dL)	82.0 (61–97)	75 (57–88)	105 (93–116)
Albumin (g/dL)	2.7 (2.3–3.1)	2.5 (2.0–2.7)	3.3 (3.2–3.4)
ALT[d] (U/L)	121 (47–327)	107 (44–605)	64 (49–305)
ALP[e] (U/L)	247 (158–973)	227 (185–473)	240 (125–542)
PV/Ao[f] ratio	0.57 (0.43–0.74)	0.52 (0.39–0.99)	0.91 (0.51–1.04)
Presence of urolith (n)	5/9	2/6	1/3
Received surgery (n)	6/9 (66.6%)	4/6 (66.6%)	2/3 (66.6%)
PVP[g] difference (mmHg)	5 (1–8)	7 (2–8)	6 (–)
Post-surgical complications (n)	0/6	1/4	0/1

[a] RG, right gastric, [b] SBA, serum bile acid, [c] BUN, blood urea nitrogen, [d] ALT, alanine aminotransferase, [e] ALP, alkaline phosphatase, [f] PV/Ao, portal vein/aorta, [g] PVP, portal venous pressure, Median (range) shown when applicable.

Figure 1-1

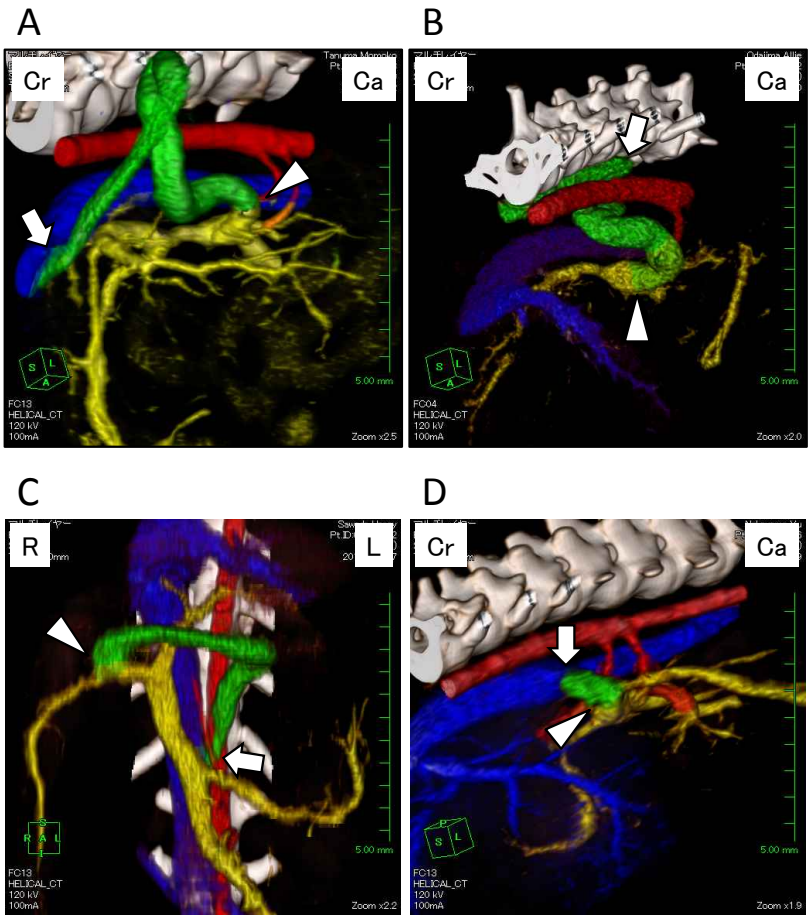

Legend for figure 1-1.

Volume rendering images of dogs with major 4 types of shunt types (red vessel, aorta; blue vessel, caudal vena cava; yellow vessel, portal vein; green vessel, shunt vessel; Cr, cranial; Ca, caudal; L, Left; R, Right). (A) Spleno-phrenic shunt as viewed from the left cranial aspect. The shunt vessel originates from the splenic vein (arrow head) and runs cranially, then drains into the caudal vena cava cranial to the liver (arrow). Note that the shunt vessel is flattened between the diaphragm and the liver. The intrahepatic portal vein was relatively sustained in this type of shunt. (B) Spleno-azygos shunt as viewed from the left cranial aspect. The shunt vessel originates from the splenic vein (arrow head) and runs dorsally with tortuous morphology, then drain into azygos vein (arrow). (C) Right gastric-caval shunt as viewed from the ventral aspect. The shunt vessel originates from the right gastric vein (arrow head) and runs laterally to the left, then drain into CVC (arrow). (D) Spleno-caval shunt as viewed from the left cranial aspect. Shunt vessel originate from the splenic vein (arrow head) then drain into CVC (arrow).

Figure 1-2

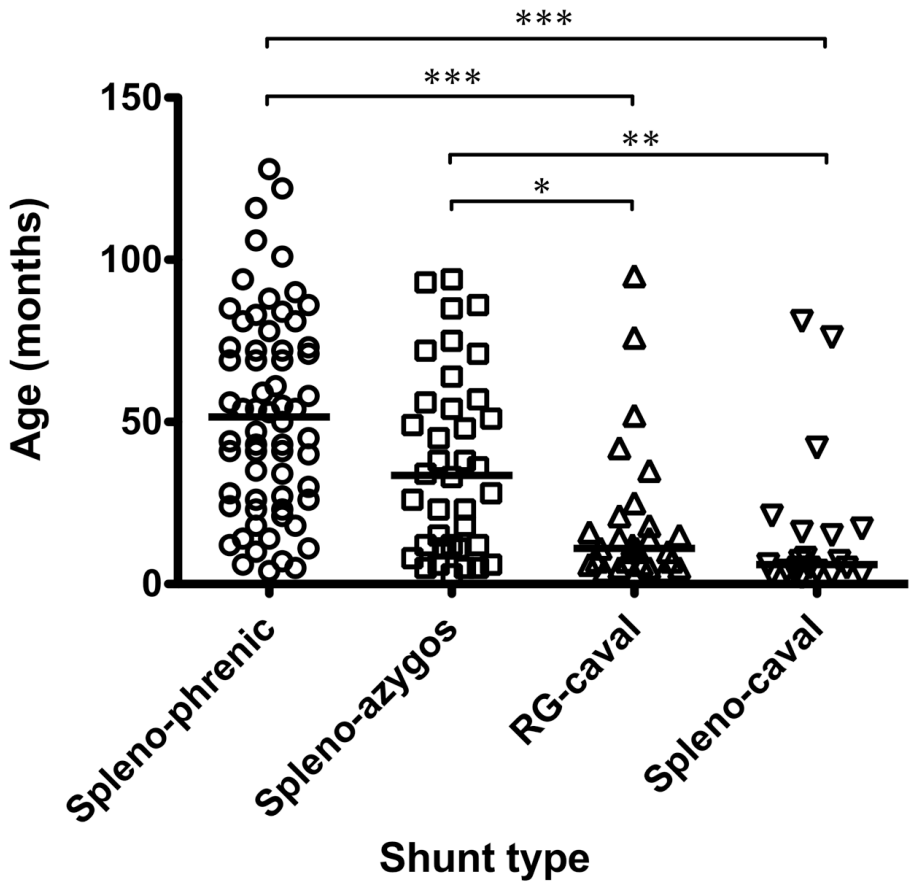

Shunt type and age at first presentation. Age at first presentation was analyzed in the four major types of the extrahepatic congenital portosystemic shunt. Spleno-phrenic and spleno-azygos shunts were diagnosed at a significantly older age than the other two shunt types. The horizontal line indicates the median.

[a] RG, right gastric

*** $P < 0.001$, ** $P < 0.01$, * $P < 0.05$

Figure 1-3

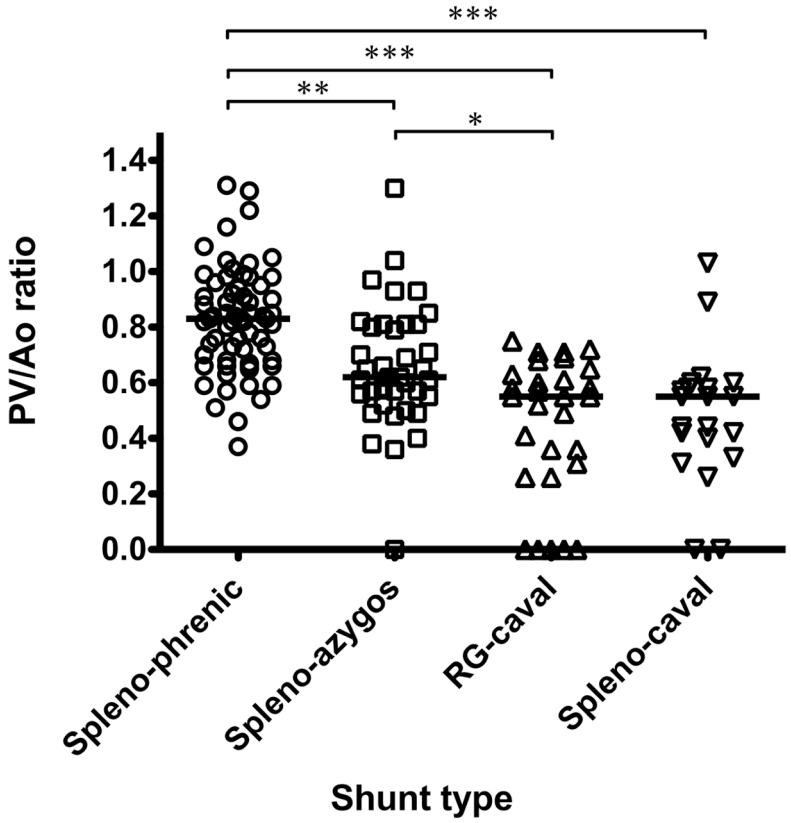

Shunt type and portal vein/aorta ratio. The portal vein/aorta (PV/Ao) ratio was analyzed in the four major types of the extrahepatic congenital portosystemic shunt. The spleno-phrenic shunt has a significantly larger PV/Ao ratio than the other shunt types, and the spleno-azygos shunt had a significantly larger PV/Ao ratio than the right gastric-caval shunt.

The horizontal line indicates the median.

[a] RG, right gastric

*** $P < 0.001$, ** $P < 0.01$, * $P < 0.05$

Figure 1-4

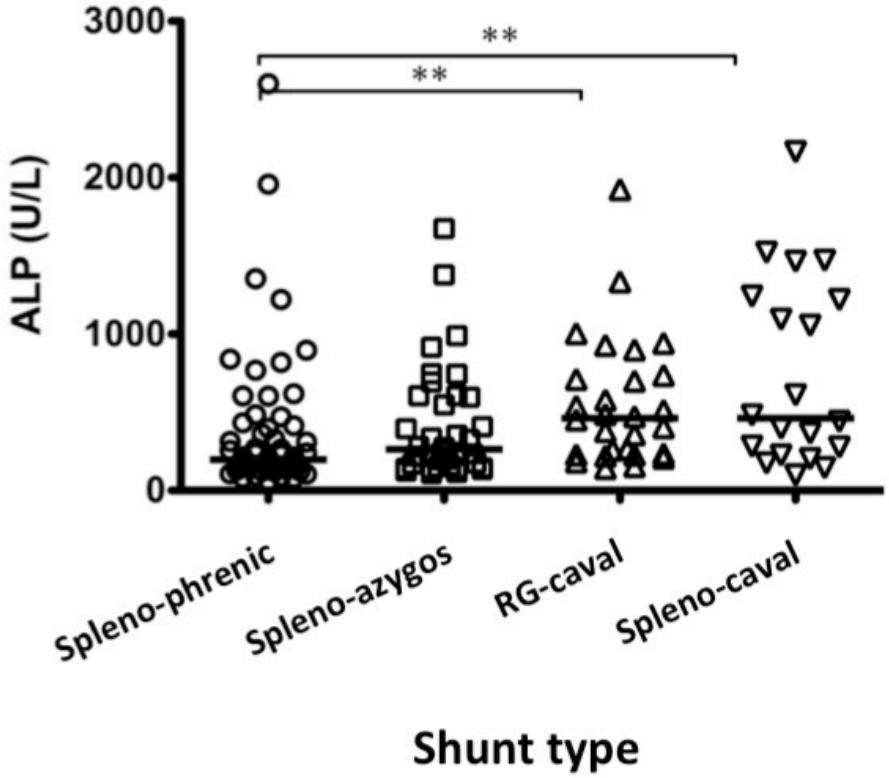

Shunt type and serum ALP activity. ALP activity was analyzed in the four major types of the extrahepatic congenital portosystemic shunt. The spleno-phrenic shunt has a significantly lower ALP level than the right gastric-caval and spleno-caval shunt.

The horizontal line indicates the median.

[a] RG, right gastric

** $P < 0.01$

Figure 1-5

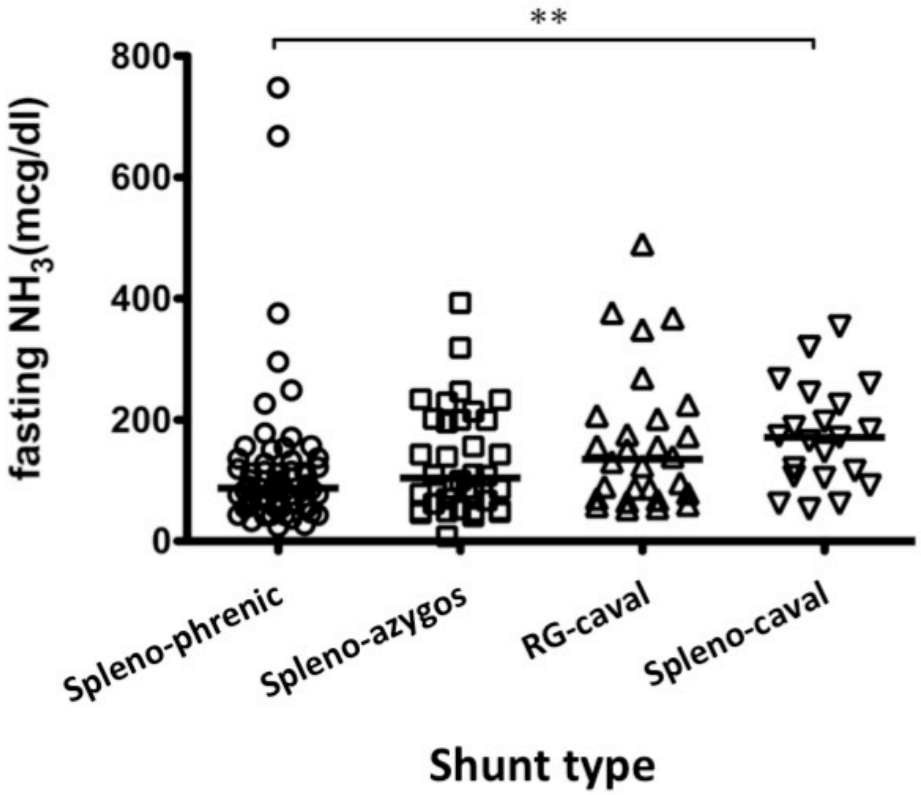

Shunt type and fasting NH_3 concentration. Fasting NH_3 concentration was analyzed in the four major types of the extrahepatic congenital portosystemic shunt. The spleno-phrenic shunt has a significantly lower fasting NH_3 concentration than the spleno-caval shunt. The horizontal line indicates the median.

[a] RG, right gastric

** $P < 0.01$

Figure 1-6

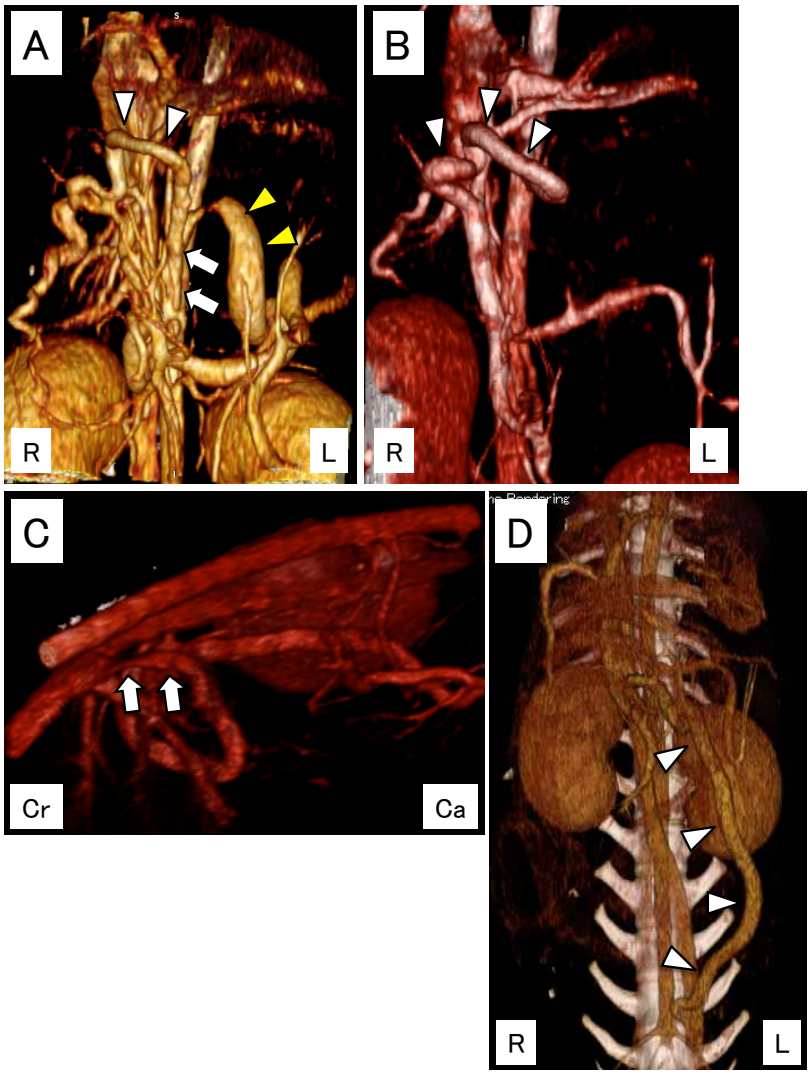

Legend for Figure 1-6.

Volume rendering images of dogs with 3 types other than major 4 types (Cr, cranial; Ca, caudal; L, Left; R, Right). (A) Right gastric-caval shunt with caudal loop as viewed from the left ventral aspect. The shunt vessel originates from the right gastric vein and runs laterally to the left (white arrow heads), join together with caudal loop originate from splenic vein (yellow arrow heads), then drains into CVC (arrows). (B) Right gastric-phrenic shunt as viewed from the ventral aspect. The shunt vessel originates from the right gastric vein (arrow heads) and runs laterally to the left side. (C) Right gastric-phrenic shunt as viewed from the left cranial aspect. The shunt vessel drain into CVC (arrows) cranial to the liver. (D) Colono-caval shunt as viewed from the ventral aspect. The colonic vein drains into CVC at caudal end of the CVC (arrow heads).

Chapter 2

Computed tomographic characteristics of hepatic mass lesions in dogs

Abstract

Little information is available on the relationship between computed tomography (CT) imaging findings and the pathologic diagnosis of canine hepatic tumors. The purpose of the study in this chapter was to clarify the characteristic features of CT findings in hepatic tumors in dogs. Data from 43 dogs with either a hepatocellular carcinoma (n = 14), hepatocellular adenoma (n = 14), nodular hyperplasia (n = 5) or other malignancies (n=10) were summarized from medical records. CT features for each hepatocellular tumor were characterized and analyzed statistically. Common findings in hepatocellular carcinoma included central (79%, $P = 0.036$) and marginal enhancement (93%, $P = 0.00043$) in the arterial phase, cyst-like lesions (93%), capsule formation (93%), and hypoattenuation in the portal (86%, $P = 0.043$), and in the equilibrium phases (93%, $P = 0.013$). Hepatic adenoma was characterized by a characteristic diffuse enhancement pattern during the arterial phase (57%, $P = 0.0013$), which was also found in nodular hyperplasia (60%), but never in hepatocellular carcinoma. Nodular hyperplasia was less likely to have a capsule structure (20%, $P = 0.0087$). Mass size was significantly smaller in nodular hyperplasia than in hepatocellular carcinoma and

hepatic adenoma (P = 0.0033 and 0.038, respectively). Hyperattenuation in the arterial and the portal phase i.e. contrast retention, was more frequent in hepatic adenoma than in the other groups (P = 0.032 and 0.032, respectively). Nodular hyperplasia was more frequently isoattenuating in the equilibrium phase (P = 0.043). In other malignancies group, all hemangiosarcoma (n=4) cases showed cyst-like lesions and hypo-attenuation in all phases. The patients with hepatic carcinoid tumor (n=2) showed contrast enhancement in the margin of the tumors in the arterial and portal phases. Findings obtained in this study will help to differentiate hepatic mass lesions in dogs using triple-phase CT examination.

Introduction

The prevalence of primary hepatic tumors in dogs is 0.6–0.9% (Patnaik *et al.*, 1980; Strombeck *et al.*, 1978). Hepatic tumors were classified into hepatocellular neoplasia, cholangiocellular neoplasia, hepatic carcinoid and hepatoblastoma, primary vascular and mesenchymal neoplasia, hematopoietic neoplasia and metastatic neoplasia (Cullen et al., 2009). Of these hepatic tumors, hepatocellular carcinoma (HCC) was the most common, followed by bile duct carcinoma, carcinoid tumor, and sarcoma. Liver tumors in dogs are classified macroscopically into massive, diffuse, and nodular tumors (Patnaik *et al.*, 1981), and are classified histologically into various types of benign and malignant tumors. Solitary or massive HCC has a good prognosis when resected completely (Liptak *et al.*, 2004; Kosovsky *et al.*, 1989), whereas dogs with other types of malignancy have a poor prognosis. Moreover, nodular hyperplasia (NH) involves benign hyperplastic nodules of hepatocellular tissues and sometimes mimics hepatic neoplasia in dogs (Cuccovillo *et al.*, 2002). In one study, 70% of necropsied dogs had

macroscopically visible NH in the liver (Bergman, 1985). Because the prognoses of benign lesions and malignant tumors are different, it is desirable to predict a precise histological of a mass-forming lesion in the liver. Liver biopsy can be used to obtain the definitive diagnosis, but it is invasive and distinguishing malignant tumor from benign liver lesions using imaging would be valuable. However, information on the relationship between histological diagnosis and CT findings is limited in small animal practice (Taniura *et al.*, 2009). Therefore, the purpose of the study in this chapter was to characterize the triple-phase CT findings in different types of hepatic mass lesions in dogs.

Materials and Methods

Case selection

Dogs that underwent abdominal helical triple-phase CT for evaluation of hepatic mass lesions (i.e. hepatocellular carcinoma (HCC), hepatocellular adenoma (HA), nodular hyperplasia (NH) and other hepatic tumors at the VMC-UTokyo between April 2005 and March 2010 were included in this retrospective study. The breed, age, sex, and body weight were obtained from the medical records. Definitive diagnosis was made histopathologically based on previously published criteria, such as the World Small Animal Veterinary Association Standards for Histological and Clinical Diagnosis of Canine and Feline Liver Diseases (Gaschen *et al.*, 2009). All of the cases were histopathologically diagnosed by an experienced pathologist. Dogs that were lacking either the data of CT images or the histopathologic specimen for reevaluation were excluded from this study.

All patients had undergone abdominal helical CT evaluation that included non-enhanced and contrast enhanced triple-phase CT through the

liver. Triple-phase CT scanning was performed as described previously with slight modification (Iseri *et al.*, 2007; Winter *et al.*, 2005). CT images were acquired with a 4-row multidetector helical CT unit (Asteion Super 4, Toshiba Medical Systems Corporation, Tochigi, Japan). The helical sequences were acquired using 120kVp and 100-150mA in a standard algorithm, with the patient was in dorsal recumbency and under general anesthesia. Slice thickness and interval was 1-3 mm with a helical pitch of 5.5. On triple-phase CT, the scan was initiated at the cranial aspect of the diaphragm and extended caudally to the level of the pelvic inlet for plain scanning, portal and equilibrium phases. In arterial phase, the scanning was extended caudally to the level of end of the liver or the mass lesion. Iohexol (300 mg I/*ml*, Omnipaque 300, Daiichi Sankyo Company. Ltd., Tokyo, Japan) was used as the contrast medium at a dose of 2 ml/kg and was injected with power injector (A-300, Nemoto Kyorindo Co. Ltd., Tokyo, Japan) over 5 to 10 seconds via jugular vein. Images were obtained before contrast medium injection, in an arterial phase (13 seconds), in a portal phase (30 seconds)

and at equilibrium phase (120 seconds) after the contrast medium injection.

Imaging analysis

Images were analyzed on OsiriX (Pixmeo, Geneva, Switzerland). Because HCC was the most frequent diagnosis in this study, I evaluated the CT findings on the basis of the past reports of CT images in human non-cirrhotic HCC (Brancatelli *et al.*, 2002).

The characteristic evaluated included number, distribution, bidirectional maximum lesion diameter, and descriptions of margins (well-defined or ill-defined) and surfaces (smooth or lobulated). A tumor capsule was defined as a thin or thick curvilinear border that surrounded at least half of the tumor and had a distinct difference in attenuation. The presence or absence of calcification was recorded. Non-enhancing areas with attenuation similar to that of the gallbladder contents were regarded as cyst-like and representative of necrosis. The presence of tumor fat was evident when the tumor components had attenuation lower than that of

water on non-enhanced CT images. Tumor thrombus was defined as distention of the hepatic and/or portal vein lumen by enhancement of the thrombus. Other findings, including dilated bile duct, and hemorrhage were assessed in accordance with a previous study (Brancatelli *et al.*, 2002). Cranial abdominal lymphadenopathy was noted when ovoid or round extravisceral masses were identified adjacent to the portal vein and had a ratio of >0.7 (short axis/long axis) (Nyman *et al.*, 2007) or when the masses had a long axis of >10 mm and a heterogeneous or ring enhancement pattern was observed (Ballegeer *et al.*, 2010). Lymph nodes were evaluated with two-dimensional transverse images of the CT.

Overall attenuation of the tumor was noted, which was defined relative to the liver parenchyma during the same phase of imaging; plain, arterial, portal, or equilibrium phase. In the assessment of overall attenuation, I ensured objectivity by measuring the CT value at the cross-section at which the lesion had bidirectional maximum diameter. If the lesion had a different CT value in Hounsfield units (HU) (>20 HU compared

with the surrounding liver parenchyma), I deemed it to be different and considered these lesions to have hyper or hypoattenuation.

Enhancement patterns of the arterial phase were evaluated in terms of 3 categories: central, marginal, and diffuse enhancement (Figure 2-1). Central enhancement was defined as blood vessels with or without dilation located in the central area of the lesion, marginal enhancement as blood vessels located along the margin, and diffuse enhancement as blood vessels extending entirely within the mass lesion.

Statistical analysis

The ratio of positivity or negativity of each finding in each lesion type was analyzed by Haberman's residual analysis. The diameter of the mass was compared among all categories by using the Steel-Dwass multiple comparison method. A P value of <0.05 was considered significant.

Results

Forty-three dogs met the inclusion criteria. There were 18 males (7 castrated) and 25 females (17 spayed). The median age and body weight were 10.5 years (range, 3 months–15 years) and 9.8 kg (range, 1.5–38.5 kg), respectively. The Affected breeds were as follows: Shih-Tzu (n=6), Golden retriever, Labrador retriever, Mix breed dog (n=4, each), Siberian husky, Beagle, Chihuahua (n=3, each), Maltase, Pomeranian, Shetland sheepdog, Pembroke Welsh Corgi, Miniature schnauzer, shiba-inu (n=2, each), Tibetan spaniel, West Highland white terrier, Italian greyhound, and Yorksher terrier (n=1, each). Histopathological diagnoses of hepatocellular tumors were HCC (n = 14), HA (n = 14), NH (n = 5). Other malignancies (OM) including hemangiosarcoma (HSA; n=4), hepatic carcinoid tumor (CND; n=2), lymphoma, lymphangiosarcoma (LSA), malignant mesenchymal tumor (MMT) and malignant peripheral nerve sheath tumor (MPNST) (1 case each). Because each case number of the OM group was too small, only hepatocellular tumors were analyzed statistically.

The CT findings of hepatocellular tumors are summarized in Tables 2-1, 2-2 and 2-3. The characteristics of HCC were large (median diameter, 105.5 mm; range, 85–165 mm) and had cyst-like or necrotic lesions (n = 13, 93%) and capsule formation (n = 13, 93%) (Table 2-1). The surface was lobulated (n = 8, 57%) or smooth (n = 6, 43%), and the margins were well defined (n = 12, 86%). Calcification (n = 3, 21%), hemorrhage (n = 2, 14%), dilated bile duct (n = 2, 14%) were observed occasionally. Cranial abdominal lymphadenopathy was noted in 5 patients (36%), and no patient had an identifiable tumor thrombus. The overall attenuation of HCC was iso (n = 7) or hypoattenuating (n = 7) in the arterial phase, but in the portal phase, most became hypoattenuating (n=12, 86%). In the equilibrium phase, hypoattenuation is significantly more frequent in HCC than in the other groups (n = 13, 93%, $P = 0.013$) (Table 2-2). On enhancement patterns in the arterial phase, central (n = 11, 79%, $P = 0.036$) and marginal (n = 13, 93%, $P = 0.00043$) enhancement were observed significantly more frequently in HCC (Table 2-3 and Figure 2-2).

The findings of HA (n = 14) were small to large (median diameter, 85.5 mm; range, 28–114 mm), most of which had well-defined margins (n = 11, 79%). Most of them showed lobulated surface (n = 12, 86%), cyst-like structures (n = 10, 71%), and capsule formation (n = 9, 64%), but they seldom had hemorrhage (n = 0, 0%), tumor fat (n = 1, 7.1%), dilated bile ducts (n = 1, 7.1%), or tumor thrombus (n = 0, 0%). Calcification (n = 2, 14%) and lymphadenopathy (n = 5, 26%) were noted in some patients. On overall attenuation, hyper-attenuation in both the arterial and the portal phase were significantly more frequent in HA (n = 4, 29%, $P = 0.032$). Out of 14 patients, eight (57%) had a diffuse enhancement pattern in the arterial phase, significantly more frequent than other lesion types ($P = 0.0013$) (Table 2-3 and Figure 2-3). As compared to the other groups, a marginal enhancement pattern was a significantly infrequent finding (29%, $P = 0.0038$, Table 2-3).

NH was significantly smaller than HCC or HA ($P = 0.0033$ and 0.038, respectively). The median diameter was 42 mm and ranged from 28 to

63 mm. Three patients had a single mass, whereas 2 had multiple masses. The surface of the mass was lobulated (n = 3, 60%) or smooth (n = 2, 40%), and most patients (n = 4, 80%) had well-defined margins. Cyst-like areas were observed in 1 patient (20%) and capsule formation was noted in 1 patient (20%), these were significantly infrequent (P = 0040 and 0.0087, respectively) (Table 2-1). Other findings, such as hemorrhage, tumor fat, dilated bile duct, tumor thrombus and calcification were not noted. Lymph node enlargement was noted in one patient (20%). On overall attenuation, isoattenuation in both the portal and equilibrium phase were observed significantly more frequently than other groups (P = 0.046 and 0.021, respectively) (Table 2-2 and Figure 2-4). In addition, hypoattenuation in the equilibrium phase is significantly less frequent than in other groups (P = 0.037). A diffuse enhancement pattern in the arterial phase was seen in 3 patients (60%).

The CT findings of OM group were summarized in Tables 2-4, 2-5. Characteristic findings of HSA including cyst like lesions (4/4) and

hypo-attenuation in all phases in triple-phase CT (Figure 2-5). CT features of CND (n=2) included multiple-mass lesions (2/2), lobulated mass (2/2), capsule formation (2/2) and lymph node enlargement (2/2). In triple-phase CT of CND cases, tumor margins were enhanced in the arterial and portal phases (Figure 2-6, 2-7). One case showed cystic lesions inside the tumor indicating necrotic lesions (Figure 2-7). Remaining cases in OM group (n=4) were lobulated (4/4), cystic (4/4), capsulated (4/4) and had multiple lesions (3/4). They showed hypo-attenuation in all phases in triple-phase CT.

Discussion

In a previous report of the CT findings of canine hepatic mass lesions (Taniura *et al.*, 2009), only 2 types, hepatocellular carcinoma and nodular hyperplasia, were investigated, and most findings were not evaluated statistically. In the study of this chapter, I evaluated the triple-phase CT findings of hepatocellular tumors classified into 3 groups (hepatocellular carcinoma, hepatic adenoma, and nodular hyperplasia) and analyze these findings statistically.

In the study of this chapter, I found that central and marginal enhancement patterns in the arterial phase were significantly more frequent in canine hepatocellular carcinoma than in the other lesions. This is consistent with the previous report in which blood vessels inside the tumor were more frequent in hepatocellular carcinoma than nodular hyperplasia (Taniura *et al.*, 2009). Other features of canine hepatocellular carcinoma included large size, cyst-like lesions, and hypo-attenuation in the portal and equilibrium phases. As hepatocellular carcinoma in dogs tends to be

diagnosed when the mass becomes large enough to cause a clinical abnormality, features such as large size and cyst-like necrotic lesions were seen commonly. It has been stated that dogs with hepatocellular carcinoma have low attenuation in the portal venous and equilibrium phases (Taniura *et al.*, 2009). These findings are comparable to the findings in this chapter of early wash out, i.e., hypo-attenuation in the portal and the equilibrium phases. Combinations of these findings might be useful for differential diagnosis of canine hepatocellular carcinoma using triple-phase CT.

A diffuse enhancement pattern in the arterial phase was observed significantly more frequent in hepatic adenoma than in other groups. This was also observed in nodular hyperplasia, whereas it was not observed in hepatocellular carcinoma. Therefore, a diffuse enhancement pattern in the arterial phase suggests a benign lesion. This enhancement pattern resembles that of hepatic adenoma and focal nodular hyperplasia in humans, which is hypervascular in the arterial phase (Hussain *et al.*, 2004; Jang *et al.*, 2009). This might reflect the difference in vascular distribution between

benign and malignant tumors. Microscopic vascular structural changes that can cause hypervascularity have been reported in human hepatic adenoma and nodular hyperplasia (Grazzioli *et al.*, 2001; Hussain *et al.*, 2004), and similar changes might occur in dogs. Because arterial hypervascularity was also reported in human patients with hepatocellular carcinoma and cirrhosis (Baron *et al.*, 2004), further investigation of this finding in dogs is needed.

In the nodular hyperplasia group, masses were significantly smaller, and cyst-like lesions and capsule formation occurred less frequently. These findings might be due to nodular hyperplasia consisting of age-associated hyperplastic nodules (Patnaik *et al.*, 1981; Strombeck *et al.*, 1996), while other tumors are proliferative lesions that result in small masses and less frequent formation of cyst-like necrotic lesions. The margin of nodular hyperplasia being demarcated by compression of the surrounding parenchyma without a fibrous capsule (Patnaik et al., 1981), explains the decreased frequency of capsule formation in CT findings. Moreover, nodular hyperplasia is more frequently iso-attenuating in the equilibrium phase.

This is similar to focal nodular hyperplasia, which is iso-attenuating in the portal and delayed phases in humans (Brancatelli *et al.*, 2002; Jang *et al.*, 2009). Although nodular hyperplasia forms small and multiple mass lesions in general (Cullen, 2009), relatively large lesions that were considered for surgery were included in this study. There is a possibility that this difference may affect the results of image findings of NH in this study.

Additionally, I described the triple-phase CT findings of other hepatic malignancies. Cases with hemangiosarcoma presented characteristic findings of cystic lesions and hypo-attenuation in all phases in triple phase CT. Hypo-attenuation in the arterial and portal phase in dogs with hemangiosarcoma has been reported previously (Kutara et al., 2013). In the present study, a case with lymphangiosarcoma showed similar features to that of hemangiosarcoma. Since hemangiosarcoma and lymphangiosarcoma are tumors of accumulating large amount of fluid (blood or lymph) inside the lesion, contrast enhancement should be weak compared to surrounding liver parenchyma. These CT findings may be useful to suspect hemangiosarcoma

or lymphangiosarcoma in the dogs with hepatic mass lesion. In two cases with hepatic carcinoid tumor, contrast enhancement in the margin of the tumor at arterial and portal phase was observed. Marginal enhancement of hepatic carcinoid tumor has been reported in a contrast ultrasonographic study (Nakamura et al., 2010). Although case number is too small, this finding might be characteristic for hepatic carcinoid tumor in dogs. Case accumulation of triple-phase CT findings of these tumors is essential to figure out useful features in differentiating these hepatic tumors.

In summary, hepatocellular carcinoma tended to show central or marginal enhancement whereas hepatic adenoma was more likely to have diffuse enhancement pattern in the arterial phase. Hypo-attenuation in the later enhancement time phase was also characteristic for hepatocellular carcinoma, whereas contrast retention in portal and equilibrium phase was characteristic for benign hepatic lesions such as hepatic adenoma and nodular hyperplasia. Hemangiosarcoma tended to show cystic lesion and hypo-attenuation in all phases in triple-phase CT. Hepatic carcinoid tumor

presented contrast enhancement in the margin of the tumor in the arterial and portal phases. These findings will help to diagnose mass lesion in the canine liver on triple-phase CT examination.

Table 2-1

Summary of the characteristic CT findings in the dogs with hepatocellular tumors

	Cyst-like	Capsule
HCC	13	13
n = 14	(93%)	(93%)
HA	10	9
n = 14	(71%)	(64%)
NH	1*	1*
n = 5	(20%)	(20%)

Each number represents the number and percentage of positive findings.

*Significantly smaller or larger compared with other cells.

HCC, hepatocellular carcinoma; HA, hepatocellular adenoma; NH, nodular hyperplasia

Table 2-2

Overall Attenuation of hepatocellular tumors in triple-phase CT

	Arterial			Portal			Equilibrium		
	Hypo	Iso	Hyper	Hypo	Iso	Hyper	Hypo	Iso	Hyper
HCC (n=14)	7	7	0*	12*	2	0*	13*	1*	0
HA (n=14)	6	4	4*	9	1	4*	9	4	1
NH (n=5)	1	3	1	2	2*	1	2*	3*	0

Numbers represent patient numbers.

*Significantly smaller or larger compared with the other groups.

HCC, hepatocellular carcinoma; HA, hepatocellular adenoma; NH, nodular hyperplasia

Hypo, hypo-attenuation; Iso, iso-attenuation; Hyper, hyper-attenuation

Table 2-3

Enhancement Pattern in the Arterial phase of hepatocellular tumors in triple-phase CT

	Enhancement pattern (%)		
	Central	Marginal	Diffuse
HCC (n = 14)	11* (79%)	13* (93%)	0* (0%)
HA (n = 14)	4 (29%)	4* (29%)	8* (57%)
NH (n = 5)	1 (20%)	2 (40%)	3 (60%)

Numbers represent patient numbers and percentages of positive findings.

*Significantly smaller or larger compared with the other groups.

HCC, hepatocellular carcinoma; HA, hepatocellular adenoma; NH, nodular hyperplasia

Table 2-4

Overall attenuation of other malignancies in triple-phase CT

	Arterial			Portal			Equilibrium		
	Hypo	Iso	Hyper	Hypo	Iso	Hyper	Hypo	Iso	Hyper
HSA (n=4)	4	0	0	4	0	0	4	0	0
CND (n=2)	0	1	1	1	0	1	1	1	0
LSA (n=1)	1	0	0	1	0	0	1	0	0
Lymphoma (n=1)	1	0	0	1	0	0	1	0	0
MMT (n=1)	1	0	0	1	0	0	1	0	0
MPNST (n=1)	1	0	0	1	0	0	1	0	0

Number represents patient numbers.

HAS, hemangiosarcoma; CND, carcinoid tumor; LSA, lymphangiosarcoma

MMT, malignant mesenchymal tumor; MPNST, malignant peripheral nerve sheath tomor

Hypo, hypo-attenuation; Iso, iso^attenuation; Hyper, hyper-attenuation

Table 2-5

Summary of the characteristic CT findings in the dogs with other hepatic malignancies

	Maximum Diameter (mm)	Cyst	Capsule	LN
HSA (n=4)	50, 68, 68, 132	4	2	3
CND (n=2)	50, 92	1	2	2
Lymphoma (n=1)	52	1	1	1
LSA (n=1)	142	1	1	0
MMT (n=1)	114	1	1	1
MPNST (n=1)	144	1	1	0

HSA, hemangiosarcoma; CND, hepatic carcinoid tumor; LSA, lymphangiosarcoma

MMT, malignang mesenchymal tumor; MPNST, malignant peripheral nerve sheath tumor

Cyst, cyst like lesion; Capsule, capsule formation; LN, lymph node enlargement

Figure 2-1

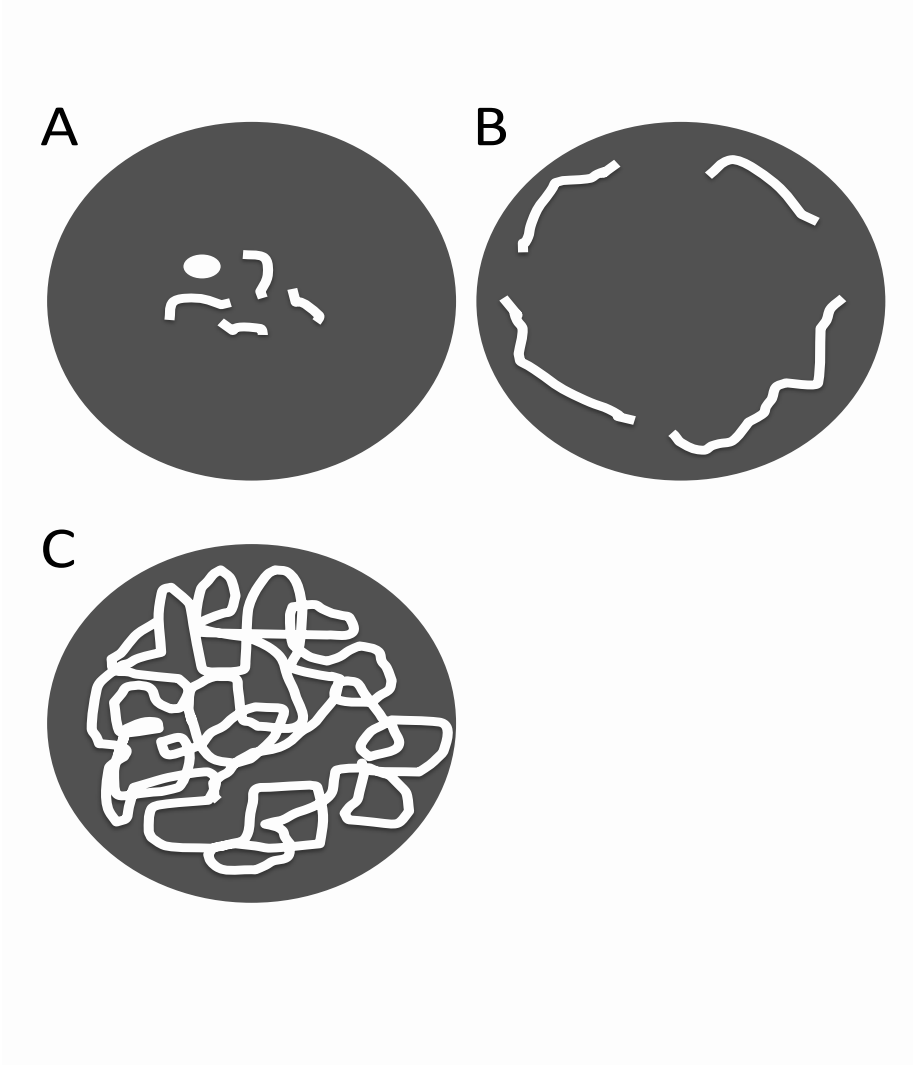

Schema of the enhancement patterns in the arterial phase. (A) Central enhancement. Blood vessels are located at the center of the lesion. (B) Marginal enhancement. Blood vessels located along the margin. (C) Diffuse enhancenment. Blood vessels extending entirely within the lesion.

Figure 2-2

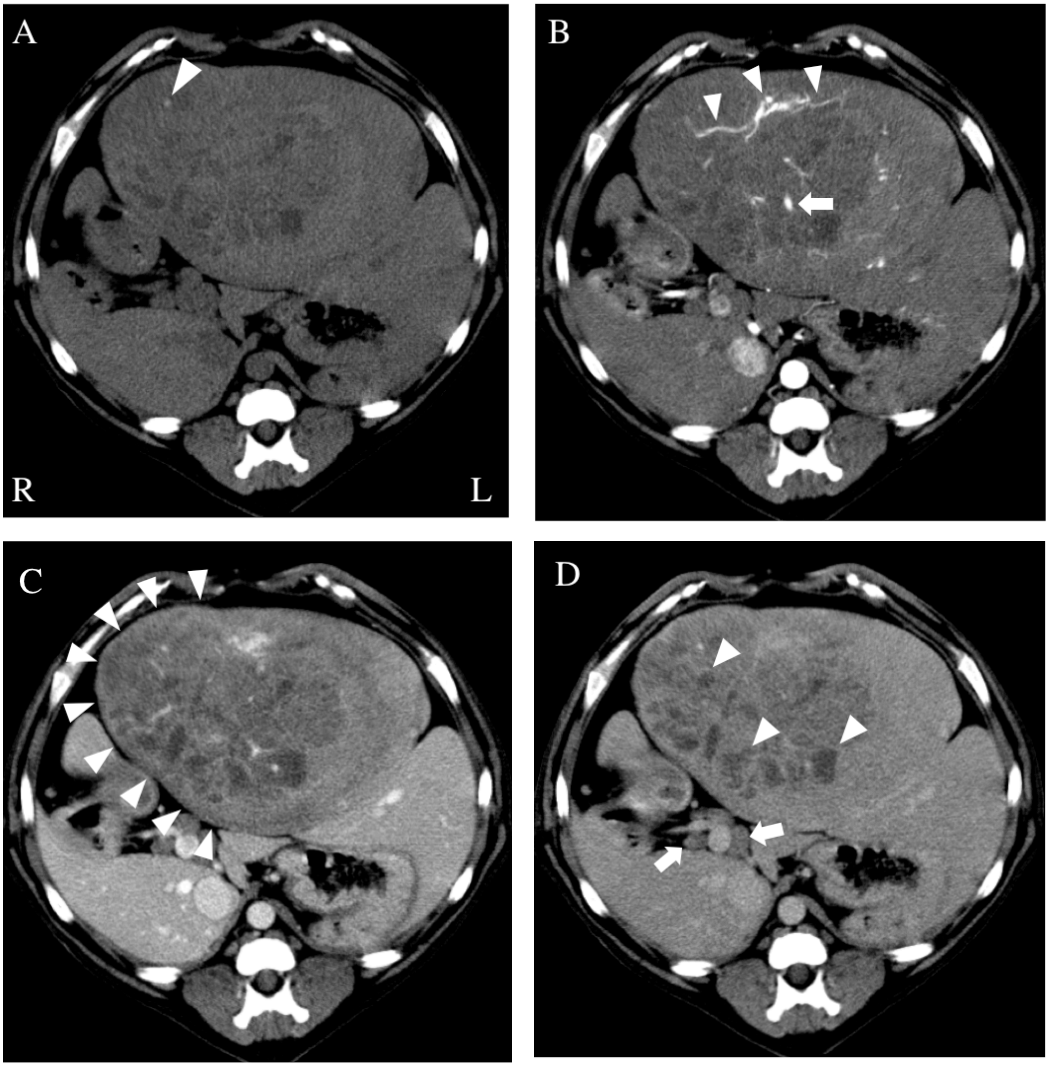

Transverse CT images of a patient with HCC. (A) Plain: Isoattenuating large mass lesion is present on the left middle lobe with calcification (arrowhead). (B) Arterial phase: Enhanced arteries are present in the center (arrow), and blood vessels are observed along the margins (arrowheads) of the tumor. (C) Portal phase: A thin, curved linear border represents the tumor capsule (arrowheads). This lesion showed hypoattenuation compared with the surrounding liver parenchyma. (D) Equilibrium phase: In the interior of the hypoattenuating mass, cyst-like lesions are observed (arrowheads). Enlarged lymph nodes are observed around the portal vein (arrows).

Figure 2-3

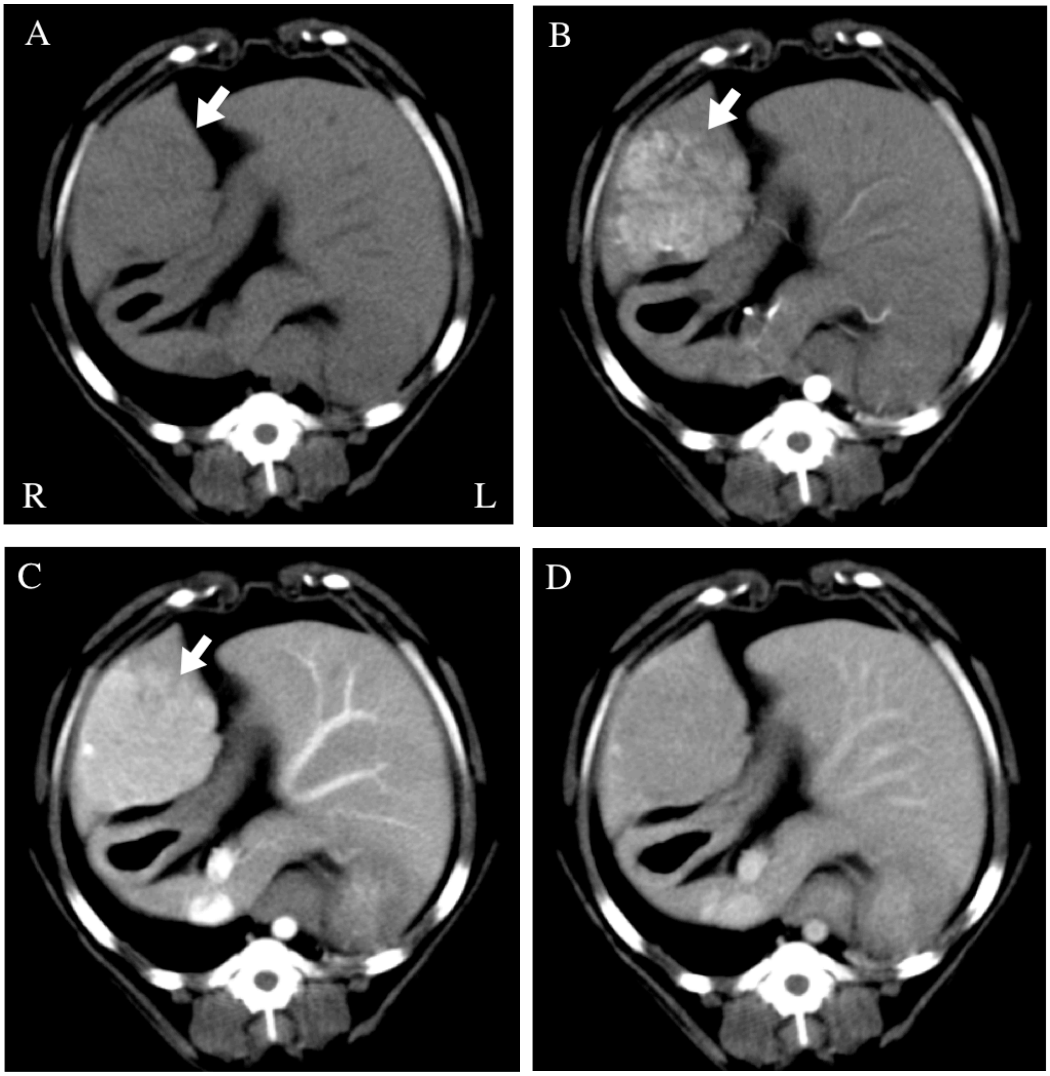

Transverse CT images of a patient with HA. (A) Plain: Isoattenuating equivocal mass lesion is observed on the right middle lobe (arrow). (B) Arterial phase: Hyperattenuating mass lesion becomes distinct with a characteristic diffuse enhancement pattern (arrow). (C) Portal phase: The lesion retains its hyperattenuation compared with the surrounding liver parenchyma (arrow). (D) Equilibrium phase: The lesion becomes isoattenuating.

Figure 2-4

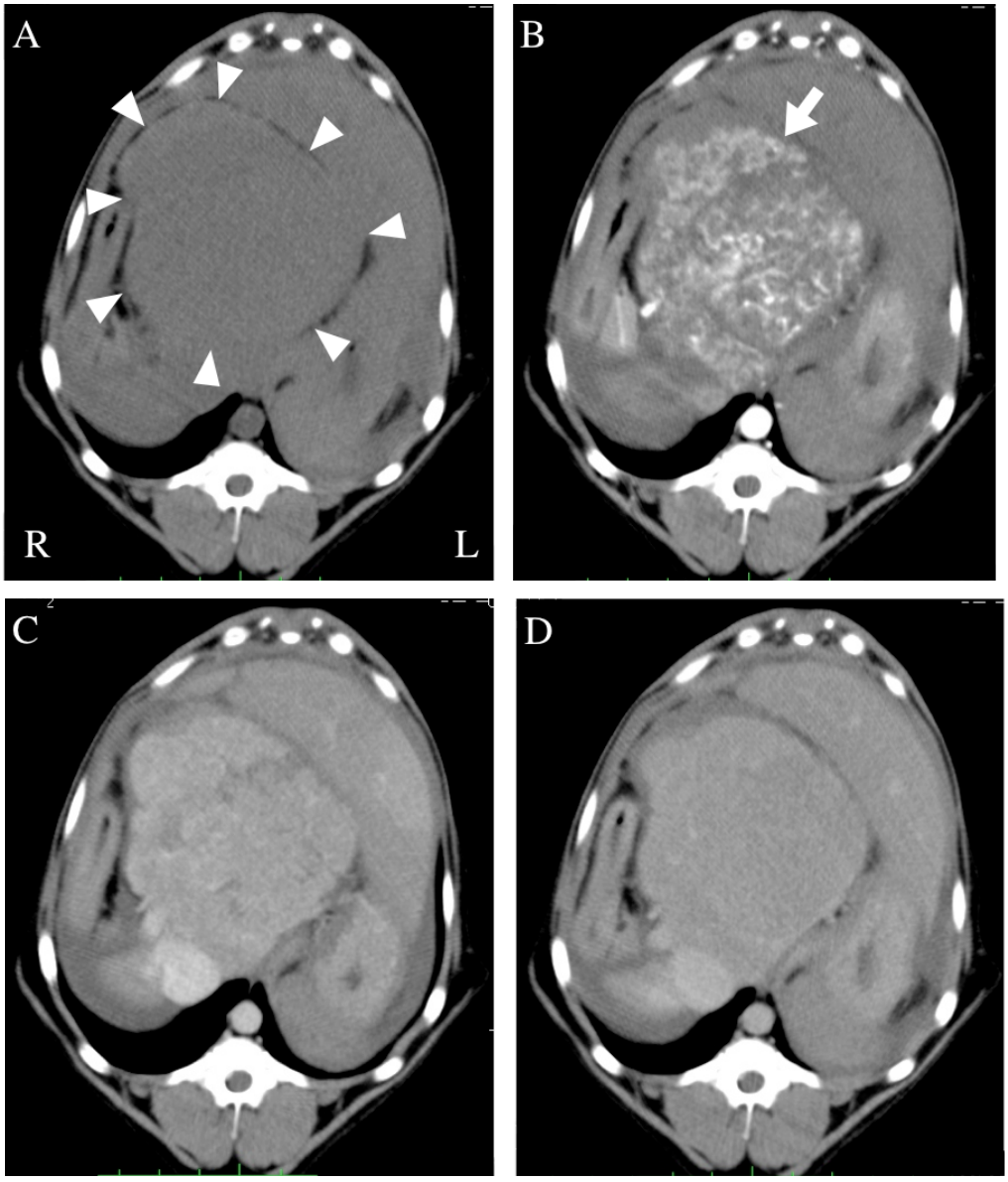

Transverse image of a patient with NH. (A) Plain: Isoattenuating mass lesion is present on the left middle lobe (arrowheads). (B) Arterial phase: The lesion shows a diffuse enhancement pattern (arrow). (C, D) Portal and equilibrium phase: The lesion shows isoattenuation.

Figure 2-5

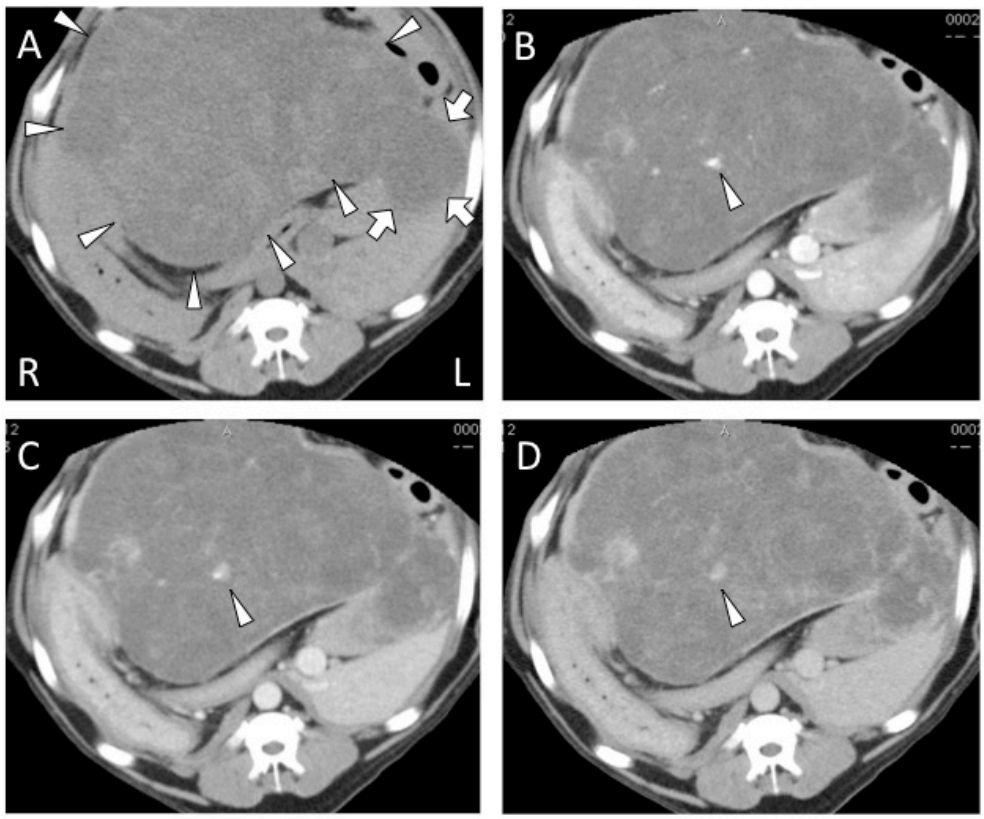

Transverse image of a patient with hemangiosarcoma. (A) Plain: Hypo-attenuating mass lesions are present on the right middle lobe (arrowheads) and left middle lobe (arrows). (B, C, D) Arterial, portal and equilibrium phase: The lesions show hypo-attenuation compared to surrounding liver parenchyma during all phases. As arterial blood supply is observed in the arterial phase (arrowhead), it gradually becomes equivocal in the later phases.

Figure 2-6

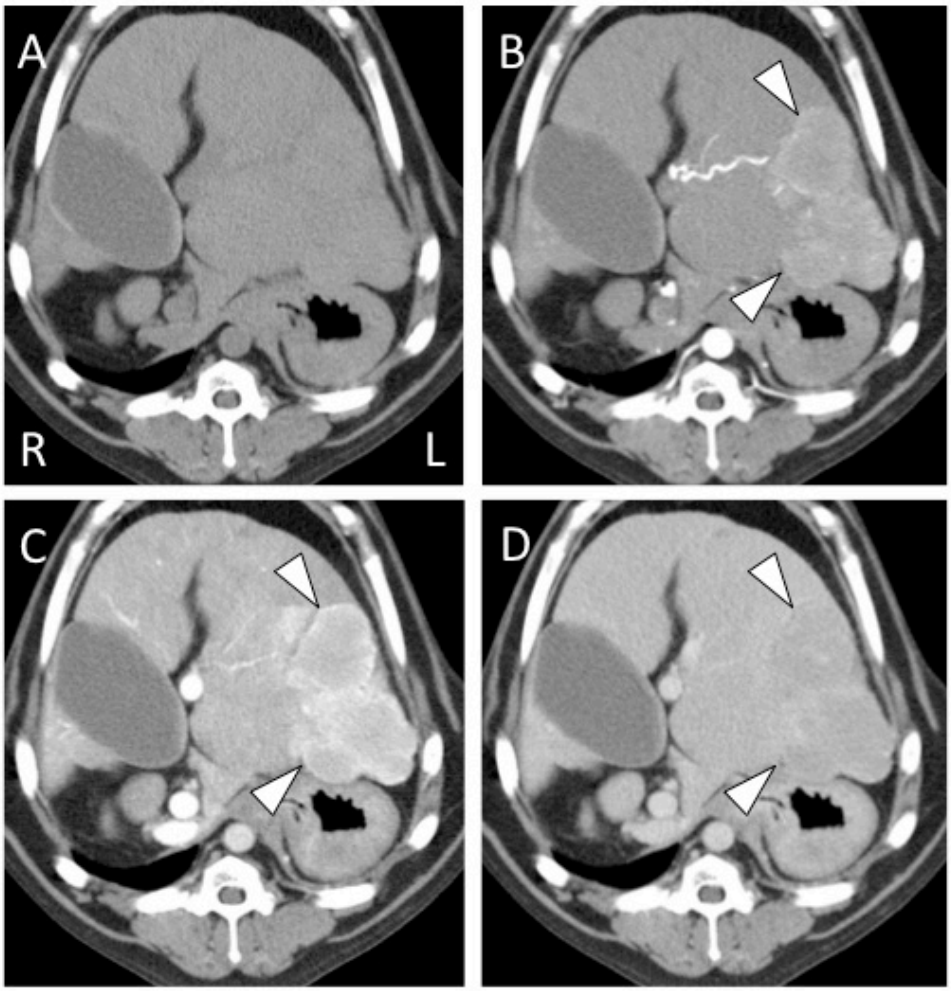

Transverse image of a patient with hepatic carcinoid tumor. (A) Plain: Since mass lesions are iso-attenuating, lesions are poorly demarcated from surrounding liver parenchyma. (B, C) Arterial and portal phase: Margin of the lesions is enhanced and lesions become extinct (arrowheads). (D) Equilibrium phase: Mass lesions become equivocal in this phase (arrowheads).

Figure 2-7

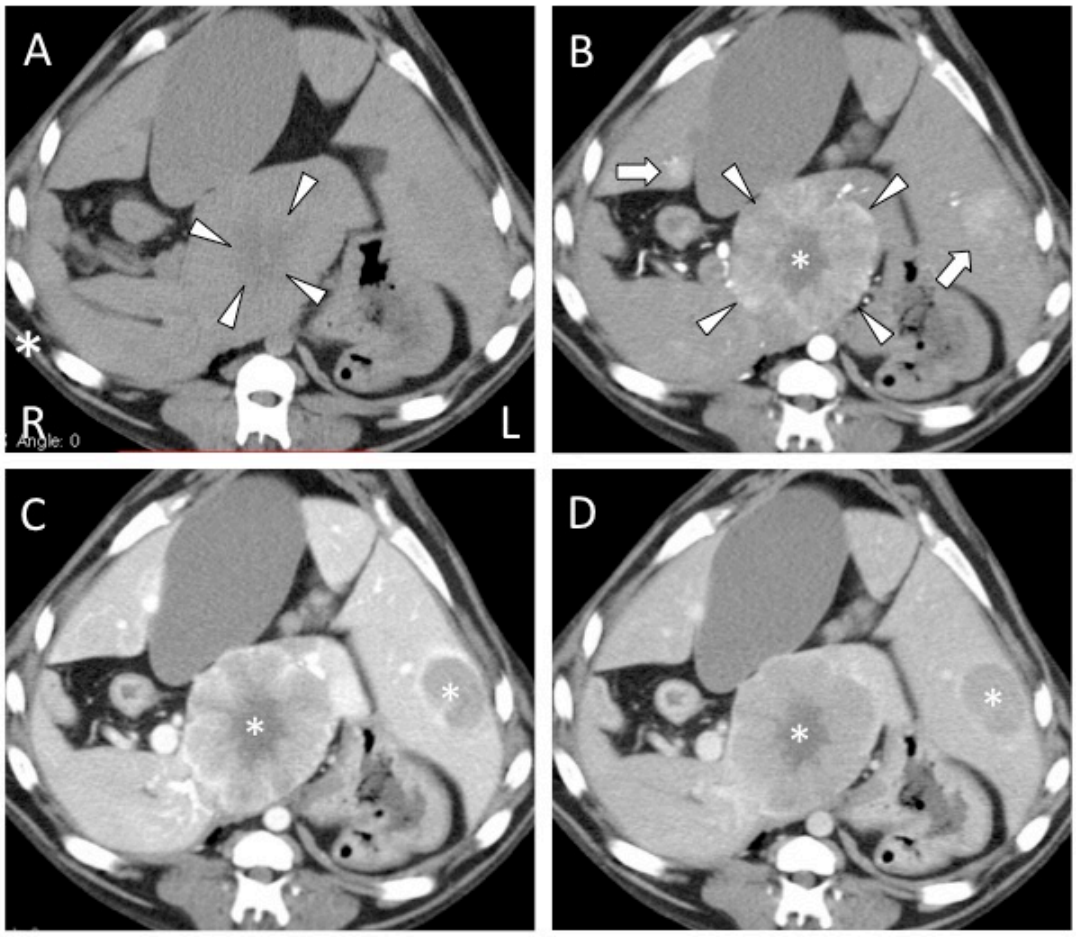

Transverse image of a patient with hepatic carcinoid tumor. (A) Plain: Hypo-attenuated lesion is observed on the caudate lobe (arrowheads). (B) Arterial phase: Mass lesion show marginal enhancement (arrowheads) with central cystic lesion (*). Additional lesions are detected on the left lateral and right middle lobe in this phase (arrows). (C, D) Portal and equilibrium phase: Mass lesions with cystic lesions show hypo-attenuation compared to surrounding parenchyma (*).

Chapter 3

Characterization of triple-phase computed tomography in dogs with pancreatic insulinoma

Abstract

Little information is available regarding triple-phase computed tomography (CT) of canine pancreatic insulinoma. A few case reports have indicated that hyper-attenuation in the arterial phase was a common finding on multi-phasic CT in dogs with insulinoma. The aim of the study in this chapter was to clarify the characteristic findings of dogs with insulinoma on triple-phase CT. Nine dogs with insuolinoma that underwent triple-phase CT were included in the present study. Attenuation patterns in the arterial phase indicated hypo-attenuation in 4 cases and hyper-attenuation in 2 cases. In the remaining 3 cases, 1 case showed hypo-attenuation and 1 case showed hyper-attenuation in the pancreatic phase, and 1 case presented hyper-attenuation in the later phase. Altogether, 5 cases showed hypo and 4 cases showed hyper-attenuation in at least one phase. The enhancement pattern was homogenous in 7 cases and heterogeneous in 2 cases. Tumor margins were well-defined in 5 cases and ill-defined in 4 cases. Capsule formation was present in 5 cases and absent in 4 cases. For the further

evaluation, histopathological features were evaluated in comparison with CT characteristics in 3 cases. While correlation between attenuation patterns (hyper or hypo attenuation) in CT and connective tissue or vascular distribution was not observed, findings of tumor margin and capsule formation in CT corresponded to histopathological features. The present study indicated that hypo-attenuation was as common as hyper-attenuation in dogs with insulinoma in triple-phase CT at least one phase. Additionally, mass lesions were most conspicuous not only in the arterial phase but in the pancreatic and later phases in some cases. Therefore, it is important to perform triple-phase CT and notice about variable findings for the detection of canine pancreatic insulinoma.

Introduction

Insulinoma is the most common pancreatic endocrine tumor in dog (Goutal *et al.*, 2012). Clinical signs are related to hypoglycemia resulting in seizure, weakness, collapse, posterior weakness, ataxia, muscle fasciculations, and lethargy. A tentative diagnosis relies on clinical signs, laboratory data such as the amended insulin glucose ratio (AIGR), and imaging diagnosis. While AIGR has high sensitivity in detection of pancreatic insulinoma in dogs, AIGR shows false positive result in hypoglycemic patient without insulin secreting tumor (Leifer *et al.*, 1986). Therefore, visualization of a pancreatic mass lesion by imaging modality is quite essential and surgical removal of the tumor is needed for both definitive diagnosis and treatment. For an imaging diagnosis, ultrasonography (US) can be used to detect a mass lesion in the pancreas (Polton *et al.*, 2007). The sensitivity of US in detecting insulinoma ranged from 28% to 75% (Lamb et al., 1995; Polton *et al.*, 2007). However, the sensitivity of insulinoma detection is depending on the operator, and various

factors such as abdominal fat, gastrointestinal gas contents, and patient characteristics can interfere with a complete examination of the pancreas. Recently, contrast-enhanced ultrasonography (CEUS) has been applied for the detection of pancreatic insulinoma in dogs (Nakamura *et al.*, 2014; Vanderperren *et al*, 2013). Although these reports describe the usefulness of CEUS with improved visualization of insulinoma lesions in dogs, this technique potentially has the same limitations described above. In contrast, computed tomography (CT) allows a full and thorough assessment of the entire pancreas. Therefore, CT is another important imaging modality for the detection of canine pancreatic insulinoma. It has been reported that conventional contrast-enhanced CT is a more sensitive imaging examination than non-contrast US or single-photon emission computed tomography (SPECT) (Robben *et al.*, 2005). Since surgical removal is the first choice for the treatment of dogs with insulinoma, CT is superior to US for insulinoma localization and staging.

In human medicine, the preoperative diagnostic utility of dual-phase

CT for pancreatic insulinoma has been well described (Gouya *et al.*, 2003; Liu *et al.*, 2009). It has been reported that this technique has promising sensitivity in the detection of insulinoma. These reports suggest that the arterial phase is important for detection; hyper-attenuation compared with the pancreatic parenchyma is a typical enhancement pattern in insulinoma. In addition, there is a report that mentioned triple-phase CT was more useful than dual-phase CT in the detection of insulinoma (Fidler *et al.*, 2003). Their report suggested that the pancreatic phase was more important than the arterial phase in detecting insulinoma.

In veterinary medicine, there have been 2 reports that described multi-phasic CT in dogs with insulinoma. The first report aimed to establish optimal enhancement conditions for pancreatic tumors in dogs on dynamic CT. In this report, 1 dog with insulinoma showed a hyper-enhanced lesion in the arterial phase (Iseri *et al.*, 2007). In the second report, 3 dogs with insulinoma underwent dual-phase CT (Mai *et al.*, 2008). While 2 cases showed hyper-attenuation in the arterial phase, the findings in 1 case were

equivocal to the surrounding pancreatic parenchyma. According to these reports, hyper-attenuation in the arterial phase may be a common finding on multi-phasic CT in dogs with insulinoma, as it is in humans. However, the number of cases was too small to draw conclusions regarding the features of multi-phasic CT in dogs with insulinoma. The purpose of the study in this chapter was to clarify the image features of dogs with insulinoma on triple-phase CT.

Additionally, histopathological features in canine insulinoma have been reported to be variable in the following aspects: invasion into the surrounding pancreatic parenchyma, condensation of connective tissue, and the presence or absence of a fibrous capsule (Capen *et al.*, 1969; Buishand *et al.*, 2010; Madarame *et al.*, 2009). As a thorough histopathological evaluation offers important information to differentiate imaging features (Capen *et al.*, 1969), comparison between the histopathological characteristics and CT findings was also carried out.

Materials and Methods

Case selection

A retrospective review of the medical records from the VMC-UTokyo was performed from April 2005 to June 2014. Inclusion criteria were as follows: (1) Dogs suspected to have pancreatic insulinoma by clinical symptoms (seizure, lethargy, and ataxia) and clinicopathological findings including increased amended insulin glucose ratio (AIGR ; > 30); (2) Dogs that underwent triple-phase CT and the data were available for reevaluation; (3) Dogs with histopahological confirmation of pancreatic insulinoma.

Clinical data including breed, age, sex, body weight, blood glucose and insulin levels, amended insulin glucose ratio (AIGR), and presence or absence of a mass lesion in the pancreas on US were collected from medical records. Histopathological findings related to metastates to regional lymph nodes or other organs were also obtained from medical records.

All patients had undergone an abdominal helical CT evaluation that included non-enhanced and contrast-enhanced triple-phase CT through the pancreas. Pancreatic triple-phase CT scanning was performed in the fixed method during the study period, which described previously with slight modification (Iseri *et al.*, 2007). In most of the cases, CT images were acquired with a 4-row multi-detector helical CT unit (Asteion Super 4, Toshiba Medical Systems Corporation, Tochigi, Japan). In the latest 1 case, image was obtained with a 80-row multi-detector helical CT unit (Aquilion Prime, Toshiba Medical Systems Corporation). The patient was in dorsal recumbency and under general anesthesia. The tube rotation speed was 1 second, slice thickness was 3 mm, and beam pitch was 0.875. The non-contrast plain CT scanning was initiated at the cranial aspect of the diaphragm and extended caudally to the level of the pelvic inlet. On arterial phase of triple-phase CT, the scan was initiated at the cranial aspect of the diaphragm and extended caudal end of pancreas. Scan area was extended caudally to the level of the pelvic inlet at pancreatic and equilibrium phase.

Iohexol (300 mg I/ml, Omnipaque 300, Daiichi Sankyo Company. Ltd., Tokyo, Japan) was used as the contrast medium at a dose of 2 ml/kg and was injected with a power injector (A-300, Nemoto Kyorindo Co. Ltd., Tokyo, Japan) over 5 to 10 sec (depending on size of the patient) via the jugular vein. Scan delay was fixed and set as 15 seconds for the arterial phase, 30 seconds for the pancreatic phase and 90 seconds for the equilibrium phase after contrast medium injection started (Iseri *et al.*, 2007).

Imaging analysis

Images were reviewed using OsiriX (Pixmeo, Geneva, Switzerland). Before image analysis, validity of each phase was assessed depending on following criteria (Fidler et al., 2003). The phase was considered as the arterial phase if there was enhancement of the arteries without enhancement of the cranial mesenteric vein. The phase was considered as the pancreatic phase if there was enhancement of the cranial mesenteric vein. The subsequent phase was classified as the later phase. If any of the

phases were not corresponded to the criteria, these cases were excluded from the present study.

The features evaluated included location, size, margin demarcation (well-defined or ill-defined) and presence of a tumor capsule. A tumor capsule was defined as a thin curvilinear border that surrounded the tumor and had a distinct difference in attenuation. Presence or absence of lymphadenopathy and hepatic nodule were evaluated.

Enhancement patterns were evaluated as homogenous or heterogeneous. The overall attenuation of the tumor was also noted, which was defined relative to the pancreatic parenchyma during the same phase of imaging (pre-contrast, arterial, pancreatic, or later phase). If the lesion had a different CT value in Hounsfield units (HU) (>20 HU compared with the surrounding pancreatic parenchyma), I deemed it to be different and considered these lesions to have hyper- or hypo-attenuation. The phase that presented the most different CT values between the lesion and pancreatic parenchyma was recorded as the most conspicuous phase.

Histopathological evaluation

When the paraffin-embedded tissue samples were available, histopathological features were reevaluated by a veterinary pathologist unaware of the CT findings. The samples were sectioned at 4 μm and stained with hematoxylin and eosin (HE) and Masson's trichrome. Immunohistochemistry was also performed by labeled streptavidin biotinylated antibody (LSAB) or by the EnVision Polymer method using goat serum against CD34 (1:80, Santa Cruz Biotechnology, CA, USA) and guinea pig polyclonal anti-insulin antibody (1:200, Dako, Glostrup, Denmark).

The proliferation of connective tissue was investigated by Masson's trichrome staining. Depending on the blue-stained area inside the lesion, the degree of connective tissue proliferation was assessed subjectively as mild, moderate, or severe. Distribution of the blood vessels was evaluated by counting CD34-positive branches. The numbers of branches were counted randomly in 5 high-power fields (×200), and then the mean and standard

deviation of the numbers of branches were calculated. Comparing these data, I classified each patient as relatively rich or poor in blood vessel distribution. I assessed the degree of capsule formation by evaluating the blue-stained area around the lesion of the Masson's trichrome-stained specimens (well-encapsulated or non-encapsulated). It is because tumor cells of insulinoma were positively stained by anti-insulin immunohistochemistry, tumor invasiveness into the surrounding tissue was evaluated by anti-insulin immunohistochemistry (invasive or noninvasive). The histopathological features were evaluated in comparison with CT findings.

Results

Nine dogs met the inclusion criteria. Clinical features of each patient are summarized in Table 3-1. The median blood glucose and insulin levels were 38 mg/dl (range, 32-50 mg/dl) and 24.2 μU/ml (1.8-312 μU/ml), respectively (Table 3-1). The median AIGR value was 200 (range, 90–3,900). Although all 9 cases underwent abdominal ultrasonography, mass lesions were identified in only 2 cases by US (22.2%). The mass lesions were detected in the right lobe in a case and in the left lobe in another case. On triple-phase CT, tumors were detected in the left lobe in 5 cases, in the right robe in 3 cases, and in the pancreatic body in 1 case. The median maximum diameter of the tumors was 12 mm (range; 9 – 20 mm).

The overall attenuation on triple-phase CT is summarized in Table 3-2. Four cases were hypo-attenuated (Figure 3-1) and other two cases were hyper-attenuated (Figure 3-2) compared with the pancreatic parenchyma at the arterial phase. One case showed hypo-attenuation and other 1 case showed hyper-attenuation at the pancreatic phase. The remaining one case

showed hyper-attenuation in the later phase. Altogether, five cases showed hypo-attenuation and four cases showed hyper-attenuation at least one phase. Of these 9 cases, 6 cases were most conspicuous in the arterial phase, 2 cases were most conspicuous in the pancreatic phase (Figure 3-3) and 1 case was most distinct in the later phase. Other CT findings are also summarized in Table 3-2. Enhancement patterns were homogenous in 7 cases and heterogeneous in 2 cases. Margins were described as well-defined in 5 cases and ill-defined in 4 cases. Capsule formation was observed in 5 cases.

Lymphadenopathy was observed in 4 cases (hepatic lymph nodes in 3 cases and splenic lymph nodes in 1 case). Of these 4 cases, a lymph node biopsy was performed in 2 cases (case Nos. 2, 6). While a case with contrast enhancement had the evidence of lymph node metastasis of insulinoma histopathologically, one case without enhancement diagnosed as lymph node hyperplasia. Although hyper-attenuated hepatic nodules were detected in one case in the arterial phase, liver biopsy was not performed and

histopathological evidence of metastasis was not confirmed in this case.

Parrafin-embedded blocks from 3 cases were available for further histopathological evaluation (case Nos 5, 8, and 9). Comparison between CT characteristics and histopathological evaluation is summarized in Table 3-3. The overall attenuation (hypo- or hyper-attenuation) and enhancement pattern (homogeneous or heterogeneous) were not histopathologically related to the severity of connective tissue proliferation or the density of blood vessels. However, patients with ill-defined tumor margins on CT corresponded to the histologic feature of invasiveness. Additionally, the presence or absence of a capsule on CT was also identical to the histopathological findings of the capsule in all 3 cases (Figure 3-4).

Discussion

In the study of this chapter, I described the image features of insulinoma on triple-phase CT in larger number of dogs than previous case reports. In previous reports of multi-phasic CT findings in canine insulinoma, an enhancement pattern of hyper-attenuation in the arterial phase was dominant (Iseri *et al.*, 2007; Mai *et al.*, 2008). However, in the present study, hypo-attenuation (4 cases) was more common than hyper-attenuation (2 cases) in the arterial phase.

It has been reported that hypo-attenuation was found as an atypical enhancement pattern in 13% of human insulinoma patients (Fidler *et al.*, 2003). The reason why hypo-attenuation is common in canine insulinoma compared to human was unknown. It has been reported that histopathological features in canine insulinoma were variable in the following aspects: invasion into the surrounding pancreatic parenchyma, condensation of connective tissue, and the presence or absence of a fibrous capsule (Buishand *et al.*, 2012; Capen *et al.*, 1969; Madarame *et al.*, 2009).

Therefore, I evaluated histopathological findings in comparison with CT characteristics in this study. Pathological features including condensation of connective tissue and vascular distribution inside the lesion were not related to enhancement pattern in the triple-phase CT. However, invasion into the surrounding parenchyma and fibrous capsule formation corresponded to the image features of margin description and present or absent of tumor capsule. Since the finding of ill demarcated margin on CT might suggest tumor invasion to surrounding parenchyma histopathologically, it is important to ensure sufficient surgical margin if the clinicians are planning to resect insulinoma. Since the number of the cases was small in this study, further case accumulation is needed to improve the utility CT examination in veterinary medicine.

In 6 out of 9 cases, mass lesions were most distinct in the arterial phase and corresponded to enhancement patterns in previous reports of dogs and humans with insulinoma (Gouya *et al.*, 2003; Iseri *et al.*, 2007; Liu *et al.*, 2009; Mai *et al.*, 2008). However, 3 out of 9 cases presented a conspicuous

mass lesion in the pancreatic or the later phase. There is a report that suggests the importance of the pancreatic phase on triple-phase CT for the detection of insulinoma in humans (Fidler *et al.*, 2003). Additionally, there is a report about CEUS in dogs with insulinoma that describes drastic changes in enhancement patterns for every moment (Nakamura *et al.*, 2014). Therefore, multi-phasic CT is essential (triple-phase must be preferred to dual-phase) to obtain adequate image for the detection of canine insulinoma. Under the triple-phase CT in the present study; however, body weight and anesthetic condition which may affect the results of enhancement pattern of the pancreatic parenchyma or the tumor lesion were not factored in. Therefore, prospective study is needed to establish a more adequate protocol for multi-phasic CT on canine insulinoma such as test injection or bolus-tracking method.

Additionally, in the present study, other CT findings of canine insulinoma demonstrated a wide variety. Seven cases presented homogenous enhancement patterns, while the other 2 cases showed heterogeneous

patterns. Capsule formation was found in 5 cases, but absent in 4 cases. These various enhancement patterns were corresponded with the variable findings in the CEUS literature reported previously (Nakamura *et al.*, 2014). It is important to note that these variable findings might be observed when we evaluate canine insulinoma on CT examinations.

Lymphadenopathy was detected in 4 cases on CT. One out of 2 cases with a lymph node biopsy showed histopathological evidence of insulinoma metastasis. Enhancement pattern was consistent with primary tumors and metastatic lymph nodes at the same phase. Another case was found to be lymph node hyperplasia in the histopathological evaluation; contrast enhancement was not observed in all phases. An enhancement patterns comparable to that of the primary lesion in the pancreas might indicate lymph node metastasis. Although there was 1 case of suspected hepatic metastasis on CT, its biopsy was not performed. As the metastatic rate of canine insulinoma has been reported as 45 to 55% at the time of diagnosis (Goutal *et al.*, 2012), it is important to carefully assess the liver and regional

lymph nodes and on CT when insulinoma is suspected.

While mass lesions in the pancreas were detected in only 2 cases by US, all of the mass lesions were detected by CT. This result corresponds to that of a previous study in which low sensitivity for the detection of canine insulinoma was reported for US (Robben *et al.*, 2005). Additionally, a CT examination allows surgeons to consider surgical resection and plan the surgical procedure. Consequently, triple-phase CT is a superior imaging modality to non contrast-enhanced US as a diagnostic tool for canine insulinoma.

The present study had several limitations. First of all, by the nature of the retrospective study, triple-phase CT in the present study was performed in fixed scan delay despite different body weight and anesthetic condition of each case. For the large breed dogs, it takes more time for injection of contrast medium than the small breed dogs. That might result in reduced intensity of CT value in the pancreatic parenchyma or the tumor lesion in the large breed dogs. It may affect the results of enhancement

pattern in the present study. To reduce these potential technical problems, more applicable method for pancreatic CT imaging should be determined such as test injection or bolus-tracking method. Second, case number was small in the present study. Further case accumulation of the triple-phase CT is needed to make more certain evidence about image findings in canine pancreatic insulinoma.

In summary, I described the characteristics of canine insulinoma on triple-phase CT in this chapter. It is important to note that hypo-attenuation in at least one phase was as common as hyper- attenuation in dogs with insulinoma in triple-phase CT. Additionally, other variable features of canine insulinoma were identified including that homogenous and heterogeneous enhancement patterns were present, descriptions of tumor margins ranged from ill-defined to well-defined, and both the presence and absence of capsule formation were observed. Although the arterial phase is essential for the detection of canine insulinoma, the pancreatic and the later phase are needed to avoid missing detection of the lesion. It is important to

be familiar with the CT findings of canine insulinoma when a patient with suspected insulinoma is evaluated by CT imaging analysis.

Table 3-1

Clinical features of the dogs with insulinoma

Case No.	Breed	Sex	Age	BW (kg)	GLU (mg/dl)	Insulin (μU/ml)	AIGR	US findings	CT findings	
									Location	Size (mm)
1	Pug	SF	8y10m	7.7	35	15.8	316	ND	Left	20
2	PWC	CM	8y3m	15.6	44	22.9	163.6	ND	Body	8.5
3	Mix	SF	7y6m	11.0	37	13.8	200	ND	Right	12
4	Maltase	SF	9y3m	3.3	32	1.8	90	ND	Left	9
5	Shi Tzu	SF	11y	6.6	34	73.9	1848	+ (left)	Left	18
6	FCR	CM	7y11m	27.7	45	55.3	368.7	ND	Left	12
7	Mix	M	9y8m	18.6	50	27.6	137.8	ND	Right	12
8	LR	CM	8y9m	33.0	38	312.0	3900	ND	Left	11
9	Toy poodle	M	11y	5.8	50	24.2	120.9	+ (right)	Right	12

PWC, Pembroke Welsh corgi; ACS, American cocker spaniel; FCR, Flat-Coated Retriever; LR, Labrador Retriever

M, male; F, female; CM, castrated male; SF, spayed female

AIGR: amended insulin glucose ratio

ND: not detected

Right, right lobe; Left, left lobe; Body, Pancreatic body

Table 3-2

CT findings in dogs with insulinoma

Case No.	Overall attenuation				Enhancement pattern	Margin description	Capsule	LN enlargement (CE)
	Non-contrast	Arterial	Pancreatic	Later				
1	Iso	Hypo*	Hypo	Hypo	Homo	Well	+	-
2	Iso	Hypo*	Iso	Iso	Homo	Ill	+	+ (-)
3	Iso	Hyper*	Iso	Iso	Homo	Well	-	+ (arterial)
4	Iso	Iso	Hyper*	Iso	Homo	Well	-	-
5	Iso	Hyper*	Iso	Iso	Hetero	Ill	-	-
6	Iso	Iso	Iso	Hyper*	Homo	Well	-	+ (later)
7	Iso	Iso	Hypo*	Hypo	Homo	Ill	+	+ (-)
8	Iso	Hypo*	Iso	Iso	Hetero	Ill	+	-
9	Iso	Hypo*	Hypo	Iso	Homo	Well	+	-

LN: lymph node

CE: contrast enhancement

Hypo, hypo-attenuation; Iso, iso-attenuation; Hyper, hyper-attenuation

Hetero, heterogenous; Homo, homogenous

+, present; -, absent

*The CT value showed the greatest difference between the lesion and pancreatic parenchyma.

Table 3-3

Comparison between CT images and histopathological findings

Case No.	CT findings				Hsitopathological findings			
	Attenuation	Pattern	Margin	Capsule	Connective tissue	Blood vessels	Invasion	Capsule
5	Hyper	Hetero	Ill	-	Severe	Poor	+	-
8	Hypo	Hetero	Well	+	Mild	Rich	-	+
9	Hypo	Homo	Well	+	Severe	Poor	-	+

Figure 3-1

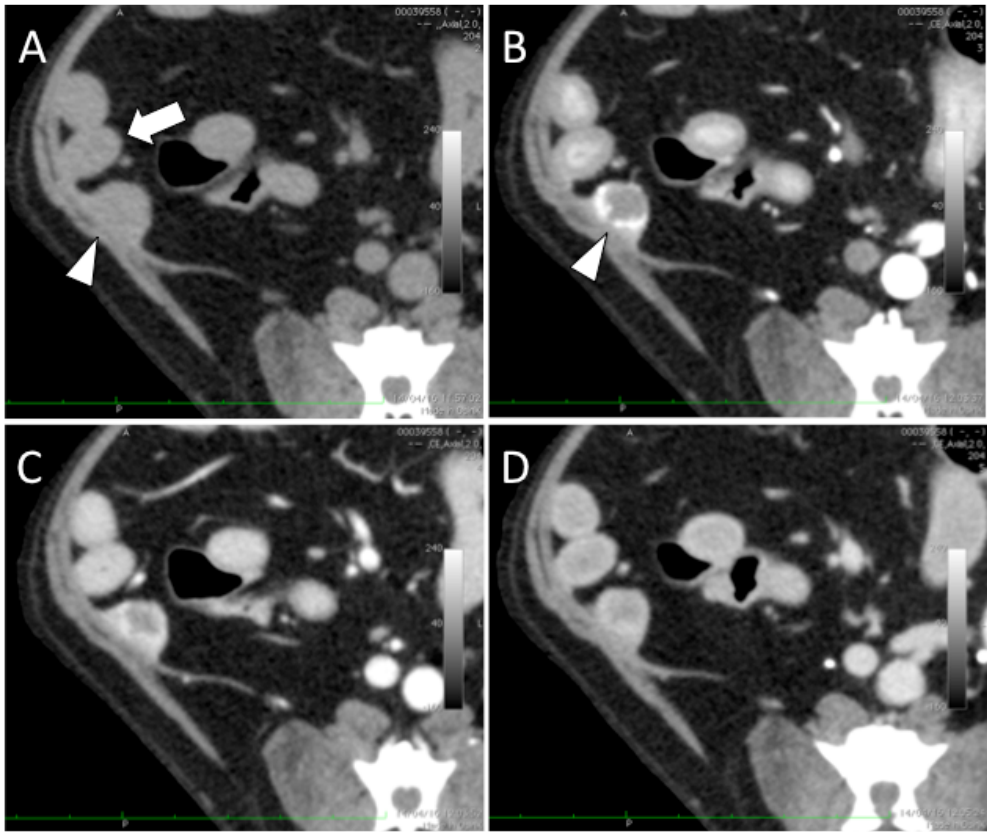

Transverse CT images of a patient with insulinoma (case 9). (A) Pre-contrast: the right lobe of the pancreas (arrowhead) was observed at the dorsal area of the duodenum (arrow). A mass lesion is not evident. (B) Arterial phase: a hypo-attenuating mass lesion with marginal ring enhancement is distinctly observed (arrowhead). The description of the margin was well-defined with a capsule. (C) Pancreatic phase: the hypo-attenuating mass lesion was still found in this phase, but gradually became equivocal. (D) Later phase: the mass lesion became more equivocal than in the early phases.

Figure 3-2

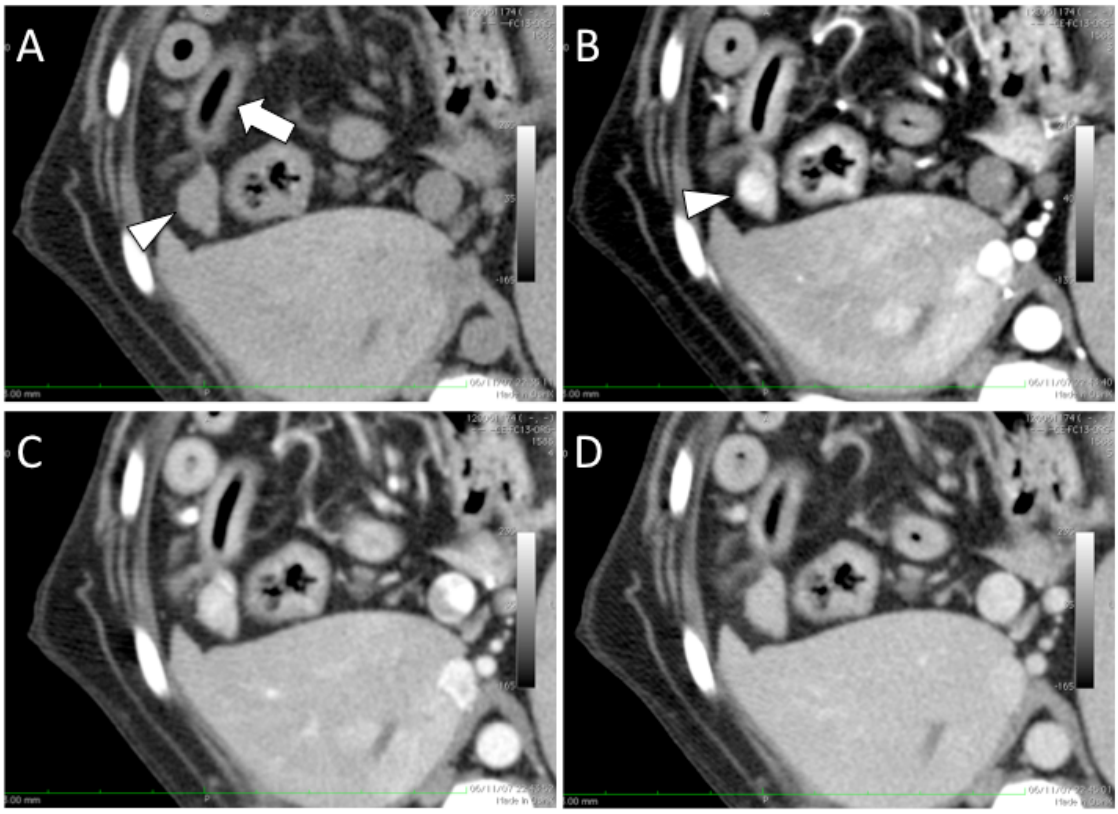

Transverse CT images of a patient with insulinoma (case 3). (A) Pre-contrast: the right lobe of the pancreas (arrowhead) was observed at the dorsal area of the duodenum (arrow). A mass lesion is not evident. (B) Arterial phase: a hyper-attenuating mass lesion is distinctly observed (arrowhead). The description of the margin was well-defined without a capsule. (C, D) Pancreatic and Later phases: the mass lesion became equivocal. It is difficult to distinguish the mass lesion from the pancreatic parenchyma.

Figure 3-3

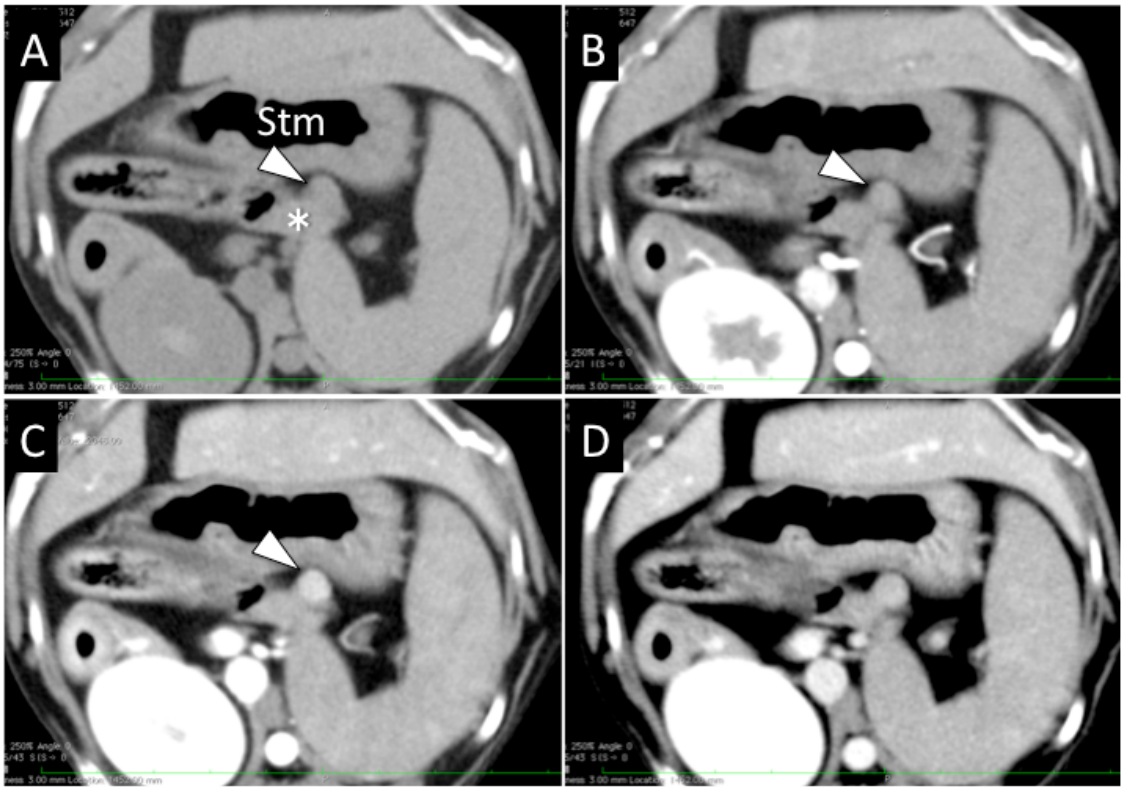

Transverse CT images of a patient with insulinoma (case 4). (A) Pre-contrast: the left lobe of the pancreas (*) was observed at the dorsal area of the stomach (stm). A raised lesion was seen, but is not evident (arrowhead). (B) Arterial phase: the mass lesion is not enhanced in this phase (arrowhead). (C) Pancreatic phase: the mass lesion is more distinctly enhanced than the pancreatic parenchyma (arrowhead). (D) Later phase: the lesion is still evident, but more equivocal than in the pancreatic phase.

Figure 3-4

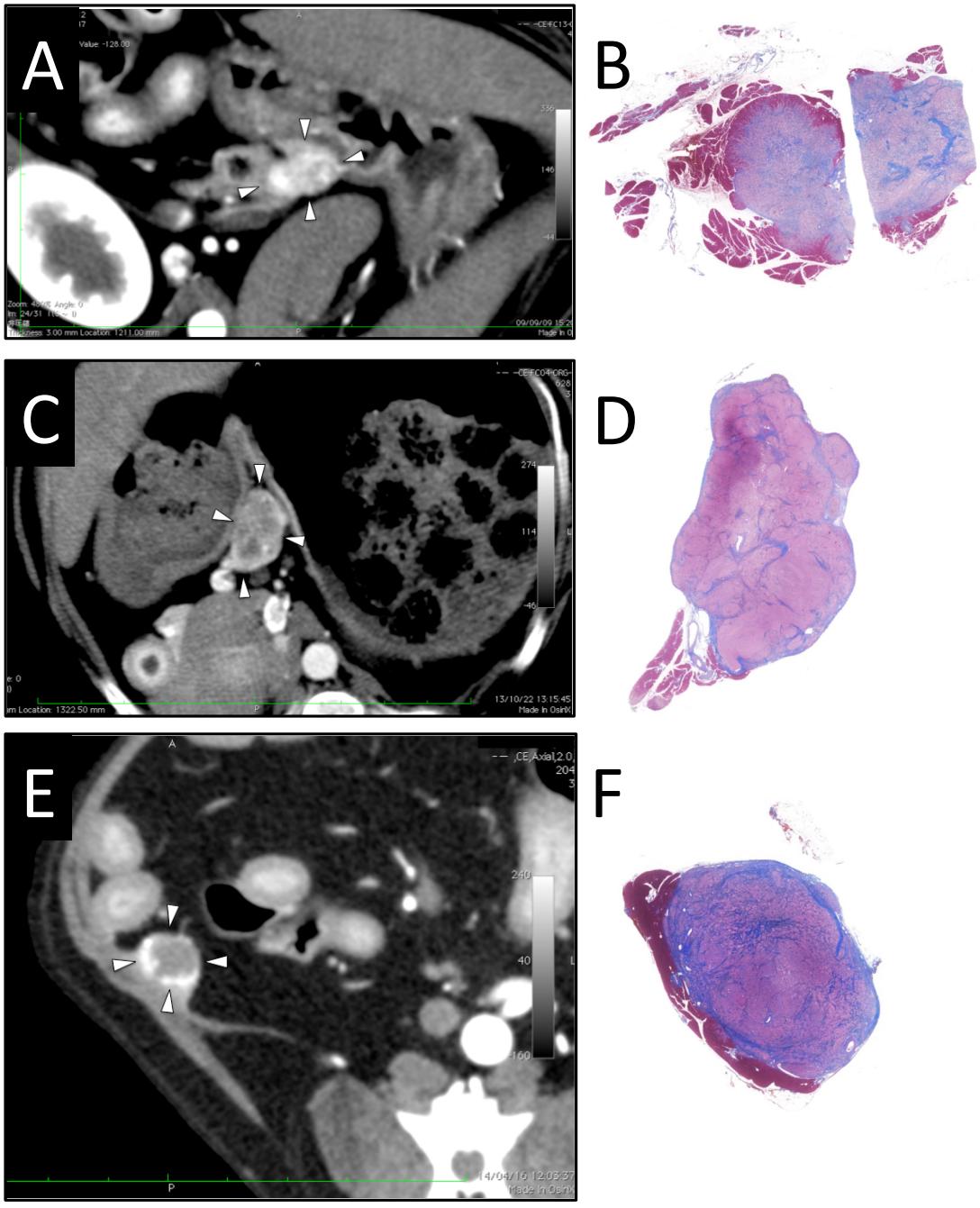

Legend for Figure 3-4

A comparison between the CT and histopathological findings. (A) Case 5. A hyper-attenuating and heterogeneous lesion is observed in the pancreatic left lobe in the arterial phase. The margin is ill-defined without capsule formation. (B) A Masson's trichrome stain of the same lesion. Connective tissue proliferation was considered severe. Tumor invasion into the surrounding tissue is observed. Histopathological capsule formation is not present. (C) Case 7. A hypo-attenuating and heterogeneous lesion is observed in the pancreatic left lobe in the arterial phase. The tumor margin is well-defined with capsule formation (arrowheads). (D) A Masson's trichrome stain of the same lesion. Connective tissue proliferation was considered mild. The tumor has a thin capsule, and invasion into the surrounding tissue was not observed. (E) Case 9. A hypo-attenuating and homogenous lesion is observed in the pancreatic right lobe in the arterial phase. The tumor margin is well-defined with capsule formation. (F) A Masson's trichrome stain of the same lesion. Connective tissue proliferation was considered severe. The tumor has a capsule, and invasion into the surrounding tissue was not observed.

Conclusion

Among several imaging modalities available in small animal medicine, CT has a potential to obtain comprehensive, objective and precise images in a relatively short time. Therefore, CT takes important part of diagnosis and classification of several hepatic and pancreatic diseases in human medicine. Although CT examination is indispensable for diagnosis and treatment planning of diseases addressed in this thesis, information regarding CT characteristics of these diseases is lacking. Therefore, I evaluated CT findings in dogs with portosystemic shunt, hepatic tumors and pancreatic insulioma to figure out the information that are useful to improve diagnostic accuracy of these diseases in this thesis.

In Chapter 1, canine extrahepatic congenital portosystemic shunts (EH-cPSS) were classified into several anatomic types, depending on their origin and termination of the shunt vessel. The aim of the study in this chapter was to determine the proportion and clinical features of each anatomical shunt type in a population of dogs presented to the VMC-UTokyo. Dogs diagnosed with EH-cPSS using CT portography were included (n = 172) and shunts were classified based on previous

reports. Clinical data were collected from case records and analyzed statistically. The most common anatomical type was the spleno-phrenic shunt (n = 64), followed by the spleno-azygos (n = 38), right gastric-caval (n = 29), spleno-caval (n = 21), right gastric-caval with caudal loop (n = 9), right gastric-phrenic (n = 6), colono-caval (n = 3), spleno-phrenic and azygos (n = 1), and porto-caval shunts (n = 1). Spleno-phrenic and spleno-azygos shunts were diagnosed significantly more frequently in older dogs than right gastric-caval and spleno-caval shunts ($P < 0.05$). The portal vein/aortic (PV/Ao) ratio was significantly larger in dogs with spleno-phrenic shunt than in dogs with the spleno-azygos, right gastric-caval or spleno-caval shunts ($P < 0.05$). The PV/Ao ratio was significantly larger in dogs with spleno-azygos shunts than in dogs with right gastric-caval shunts. Dogs with spleno-phrenic shunts had significantly lower serum alkaline phosphatase activities than those with right gastric-caval or spleno-caval shunts. Dogs with spleno-phrenic shunts had significantly lower fasting ammonia concentrations than those with spleno-caval shunts. Since several clinical features evaluated in this chapter were significantly different depending on shunt types,

thorough evaluation of shunt morphology by using CT portography is essential for the diagnosis of EH-cPSS in dogs.

In Chapter 2, the utility of triple-phase CT in differentiating hepatic mass forming lesions was described. Little information is available on the relationship between CT imaging findings and the pathologic diagnosis of canine hepatic tumors. The purpose of the study in this chapter was to clarify the characteristic features of CT findings in hepatic tumors in dogs. Data from 43 dogs with either a hepatocellular carcinoma (n = 14), hepatocellular adenoma (n = 14), nodular hyperplasia (n = 5), or other malignancies (n=10) were summarized from medical records. CT features for each hepatocellular tomor were characterized and analyzed statistically. Common findings in hepatocellular carcinoma included central (79%, P = 0.036) and marginal enhancement (93%, P = 0.00043) in the arterial phase, cyst-like lesions (93%), capsule formation (93%), and hypoattenuation in the portal (86%, P = 0.043), and in the equilibrium phases (93%, P = 0.013). Hepatic adenoma was characterized by a characteristic diffuse enhancement pattern during the arterial phase (57%, P = 0.0013), which was also found in nodular hyperplasia (60%), but never in

hepatocellular carcinoma. Nodular hyperplasia was less likely to have a capsule structure (20%, $P = 0.0087$). Mass size was significantly smaller in nodular hyperplasia than in hepatocellular carcinoma and hepatic adenoma ($P = 0.0033$ and 0.038, respectively). Hyperattenuation in the arterial and the portal phase i.e. contrast retention, was more frequent in hepatic adenoma than in the other groups ($P = 0.032$ and 0.032, respectively). Nodular hyperplasia was more frequently isoattenuating in the equilibrium phase ($P = 0.043$). In other malignancies group, all hemangiosarcoma (n=4) cases showed cyst-like lesions and hypo-attenuation in all phases. The patients with hepatic carcinoid tumor (n=2) showed contrast enhancement in the margin of the tumors in the arterial and portal phases. These findings will help to differentiate mass lesions in the canine liver on triple-phase CT examination.

In Chapter 3, characteristics on triple-phase CT in canine pancreatic insulinoma were described. No information regarding triple-phase CT of canine pancreatic insulinoma was available before this study. A few case reports indicated that hyper-attenuation in the arterial phase was a common finding on multi-phasic CT in dogs with insulinoma.

The aim of the study in this chapter was to clarify the characteristic findings of dogs with insulinoma on triple-phase CT. Nine dogs with insuolinoma that underwent triple-phase CT were included in the present study. Attenuation patterns in the arterial phase indicated hypo-attenuation in 4 cases and hyper-attenuation in 2 cases. In the remaining 3 cases, 1 case showed hypo-attenuation and 1 case showed hyper-attenuation in the pancreatic phase, and 1 case presented hyper-attenuation in the later phase. Altogether, 5 cases showed hypo and 4 cases showed hyper-attenuation in at least one phase. The enhancement pattern was homogenous in 7 cases and heterogeneous in 2 cases. Tumor margins were well-defined in 5 cases and ill-defined in 4 cases. Capsule formation was present in 5 cases and absent in 4 cases.

For the further evaluation, histopathological features including condensation of connective tissue, vascular distribution, invasiveness to surrounding tissue, and capsule formation were evaluated in comparison with CT characteristics in 3 cases. While correlation between attenuation

patterns (hyper or hypo attenuation) in CT and connective tissue or vascular distribution was not observed, findings of tumor margin (well or ill demarcated) and capsule formation (present or absent) in CT corresponded to their histopathological features.

The study in chapter indicated that hypo-attenuation was as common as hyper-attenuation in dogs with insulinoma in triple-phase CT at least one phase. Additionally, mass lesions were most conspicuous not only in the arterial phase but in the pancreatic and later phases in some cases. Therefore, it is important to perform triple-phase CT and notice about variable findings for the detection of canine pancreatic insulinoma.

In summary, I described in this thesis a series of clinically important CT findings for classification as well as detection and differentiation of hepatic and pancreatic diseases in dogs. The study in the Chapter 1 revealed that spleno-phrenic and spleno-azygos shunts are common types of canine EH-cPSS in Japan and they had specific clinical features such as being diagnosed at relatively older age and having sustained PV/Ao ratio. It is

important for the clinicians to notice about these facts. Since sustained PV/Ao ratio makes it difficult to detect EH-cPSS by using WSAVA standardized US procedure, novel US procedures that can detect these types of EH-cPSS are needed especially in Japan. By analyzing the CT portographic images in this chapter, it may be possible to develop new ultrasonographic diagnostic procedures for EH-cPSS consequently improving diagnostic accuracy of EH-cPSS in dogs. The study in the Chapter 2 revealed CT imaging characteristics to differentiate hepatic tumors in dogs. Since similar research results have been accumulated in recent years, it may be possible to make a differential algorithm for canine hepatic tumors by combining the results in this chapter and reported results of multi-phasic CT. I am convincing that these results are helpful to ameliorate accuracy of differential diagnosis of hepatic tumors in triple-phase CT prior to surgical intervention. Finally, the study in the Chapter 3, I described novel CT findings in the pancreatic insulinoma such as hypo-attenuation of the lesions of pancreatic insulinoma in triple-phase CT. Although I could not clarify the

mechanism of this finding histopathologically, it is important for veterinarians to notice about this finding when evaluating CT findings in the dogs with insulinoma.

One of the biggest disadvantages of CT examination in small animal practice is need for anesthesia to keep the patients immobile. Recently, the development of multi-detector low CT brings high-speed imaging into reality. This technical innovation allows veterinarians to choose unanesthetized CT. Since the sharpness of the images obtained from unanesthetized CT is inferior to that from anesthetized CT, diagnostic utility is dependent on the quality of the images. As I described some specific findings of the hepatic and pancreatic diseases in dogs, these information will contribute for interpretation of images from unanesthetized CT in seriously ill dogs suffering from these diseases in near future.

In conclusion, a series of studies on CT examination for the hepatic and pancreatic disorders in dogs will contribute to accurate diagnosis and most

suitable therapeutic strategies in each patient, providing clinically useful progress in the field of veterinary diagnostic imaging.

Acknowledgements

I would like to express my deepest gratitude to Dr. Hajime Tsujimoto and Dr. Koichi Ohno for great support and advice during this study. I also would like to express my profound gratitude to Drs. Ryohei Nishimura, Reina Fujiwara, Kazuyuki Uchida, Naoaki Matsuki, Yasuhito Fujino, Ko Nakashima, Masashi Takahashi, Hideyuki Kanemoto and Masaya Tsuboi for support of my works. I would like to acknowledge the substantial help from Miss. Kie Yamamoto.

I wish to thank all the patients and their owners in my works and all the staffs in Veterinary Medical Center of the University of Tokyo and the Department of Veterinary Internal Medicine.

Finally, I am most grateful to my family. My father, Mr. Kenji Fukushima, he is the most brave person I have ever seen and is the man who taught me how interesting it is to know something new. My mother, Mrs. Keiko Fukushima, she always devotedly supports us and becomes the ground of our families. My precious wife, Mrs. Ayano Fukushima, she provides me a great support and helps me at all times. My sweet daughter

Rino Fukushima and my dear dog Gris, they always make me smile and deprive daily stress away from me.

References

Ballegeer, E.A., Adams, W.M., Dubielzig, R.R., Dubieizig, R.R., Paoloni, M.C., Klauer, J.M., Keuler, N.S., 2010. Computed tomography characteristics of canine tracheobronchial lymph node metastasis. Veterinary Radiology & Ultrasound 51, 397-403.

Baron, R.L., Brancatelli, G., 2004. Computed tomographic imaging of hepatocellular carcinoma. Gastroenterology 127, 133-143.

Bergman, J.R., 1985. Nodular hyperplasia in the liver of the dog: An association with changes in the Ito cell population. Veterinary Pathology 22, 427-438.

Bertolini, G., 2010. Acquired portal collateral circulation in the dog and cat. Veterinary Radilogy & Ultrasound 51, 25-33.

Brancatelli, G., Federle, M.P., Grazioli, L., Carr, B.I., 2002. Hepatocellular carcinoma in noncirrhotic liver: CT, clinical, and pathologic findings in 39 U.S. residents. Radiology 222, 89-94.

Brancatelli, G., Federle, M.P., Katyal, S., Kapoor, V., 2002. Hemodynamic characterization of focal nodular hyperplasia using three-dimensional volume-rendered multidetector CT angiography. American Journal of Roentgenology 179, 81-85.

Buishand, F.O., Kik, M., Kirpensteijn, J., 2010. Evaluation of clinico-pathological criteria and the Ki67 index as prognostic indicators in canine insulinoma. The Veterinary Journal 185, 62-67.

Capen, C.C., Martin, S.L., 1969. Hyperinsulinism in dogs with neoplasia of the pancreatic islets. A clinical, pathologic, and ultrastructural study. Veterinary Pathology 6, 309-341.

Center, S.A., 1996. Hepatic Vascular Diseases. In: Guilford, W.G., Center, S.A., Strombeck, R.D., Williams, D.A., Meyer, D.J., Small Animal Gastroenterology 3rd ed. W. B. Saunders, Philadelphia, pp. 802-846.

Choi, J.Y., Lee, J.M., Sirlin, C.B., 2014. CT and MR imaging diagnosis and staging of hepatocellular carcinoma. Part I, Development, growth, and spread: Key pathologic and imaging aspects. Radiology 272, 635-654.

Choi, J.Y., Lee, J.M., Sirlin, C.B., 2014. CT and MR imaging diagnosis and staging of hepatocellular carcinoma. Part II, Extracellular agents, hepatobiliary agents, and ancillary imaging features. Radiology 273,

30-50.

Choi, S.Y., Choi H.J., Lee K.J., Lee, Y.W., 2015. Establishment of optimal scan delay for multi-phase computed tomography using bolus-tracking technique in canine pancreas. The Journal of Veterinary Medical Science 77, 1049-1054.

Cuccovillo, A., Lamb, C.R., 2002. Cellular features of sonographic target lesions of the liver and spleen in 21 dogs and a cat. Veterinary Radiology & Ultrasound 43, 275-278.

Cullen, J.M., 2009. Summary of the World Small Animal Veterinary Association standardization committee guide to classification of liver disease in dogs and cats. Veterinary Clincs of North America Small Animal Practice 39, 395-418.

D'anjou, M.A., Pennink, D., Cornejo, L., Pibarot, P., 2004. Ultrasonographic diagnosis of portosystemic shunting in dogs and cats. Veterinary Radiology & Ultrasound 45, 424-437.

de la Santa, L.G., Perez Retortillo, J. A., Miguel, A. C., Klein, L. M., 2014. Radiology of pancreatic neoplasms: An update. World Journal of Gastrointestinal Oncology 6, 330-343.

Fernandez, N.J., Kidney, B.A., 2007. Alkaline phosphatese: beyond the liver. Veterinary Clinical Pathology 36, 223-233.

Fidler, J.L., Fletcher, J.G., Reading, C.C., Andrews, J.C. Thompson, G.B., Grant, C.S., Service, F.J., 2003. Preoperative detection of pancreatic insulinomas on multiphasic helical CT. American Journal of Radiology 181, 775-780.

Frank, P., Mahaffey, M., Egger, C., Cornell, K.K., 2003. Helical computed tomographic portography in ten normal dogs and ten dogs with a portosystemic shunt. Veterinary Radiology & Ultrasound 44, 392-400.

Furlow, B.A., 2015. Computed tomography of pancreatitis and pancreatic cancer. Radiologic Technology 86, 645-668.

Gaschen, L., 2009. Update on hepatobiliary imaging. Veterinary Clincs of North America Small Animal Practice 39, 439-467.

Gerritzen-Bruning, M.J., van den Ingh, T.S.G.A.M., Rothuizen, J., 2006. Diagnostic value of fasting plasma ammonia and bile acid

concentrations in the identification of portosysmic shunting in dogs. Journal of Veterinary Internal Medicine 20, 13-19.

Goutal, C. M., Brugmann, B. L., Ryan, K. A., 2012. Insulinoma in dogs: a review. Journal of American Animal Hospital Association 48, 151-163.

Gouya, H., Vignaux, O., Augui, J., Dousset, B., Palazzo, L., Louvel, A., Chaussade, S., Legmann, P., 2003. CT, endoscopic sonography, and a combined protocol for preoperative evaluation of pancreatic insulinomas. American Journal of Radiology 181, 987-992.

Grazioli, L., Federle, M.P., Brancatelli, G., Ichikawa, T., Olivetti, L., Blachar, A., 2001. Hepatic adenomas: Imaging and pathologic findings. Radiographics 21, 877-892.

Hattori, Y., Gabata, T., Zen, Y., Mochizuki, K., Kitagawa, H., Matsui, O., 2010. Poorly enhanced areas of pancreatic adenocarcinomas on late-phase dynamic computed tomography comparison with pathological findings. Pancreas 39, 1263-1270.

Hussain, S.M., Terkivatan, T., Zondervan, P.E., Lanjouw, E., de Rave, S., Ijzermans, J.N., de Man, R.A., 2004. Focal nodular hyperplasia: findings at State-of-the-Art MR imaging, US, CT, and pathologic analysis. Radiographics 24, 3-17.

Iseri, T., Yamada, K., Chijiwa, K., Nishimura, R., Matsunaga, S., Fujiwara, R., Sasaki, N., 2007. Dynamic computed tomography of the pancreas in normal dogs and in a dog with pancreatic insulinoma. Veterinal Radiology & Ultrasound 48, 328-331.

Jang, H.J., Yu, H., Kim, T.K. Imaging of focal liver lesions. 2009, Seminars in Roentgenology 44, 266-282.

Kanemoto, H., Ohno, K., Nakashima, K., Takahashi, M., Fujino, Y., Nishimura, R., Tsujimoto, H., 2009. Characterization of canine focal liver lesions with contrast-enhanced ultrasound using a novel contrast agent-sonazoid. Veterinary Radiology & Ultrasound 50, 188-194.

Kosovsky, J.E., Manfra-Marretta, S., Matthiesen, D.T., et al. 1989. Results of partial hepatectomy in 18 dogs with hepatocellular carcinoma. Journal of the American Animal Hospital Association 25, 203-206.

Kutara, K., Seki, M., Ishikawa, C., et al., 2013. Triple-phase helical

computed tomogramphy in dogs with hepatic masses. Veterinary Raidiology & Ultrasound 55, 7-15.

Lamb, C.R., Simpson, K.W., Boswood, A., Matthewman, L.A., 1995. Ultrasonography of pancreatic neoplasia in the dog: a retrospective review of 16 cases. Veterinary Record 137, 65-68.

Lee, Y.J., Lee, J.M., Lee, J.S., Park, B.H., Kim, Y.H., Han, J.K., Choi, B.I., 2015. Hepatocellular carcinoma: diagnostic performance of multidetector CT and MR imaging – A systematic review. Radiology 275, 97-109.

Leifer, C.E., Peterson, M.E., Matus, R.E., 1986. Insulin-secreting tumor: diagnosis and medical and surgical management in 55 dogs. Journal of American Veterinary Medical Association 188, 60-64.

Liptak, J.M., Dernell, W.S., Monnet, E., Powers, B.E., Bachand, A.M., Kenney, J.G., Withrow, S.J., 2004. Massive hepatocellular carcinoma in dogs: 48 cases (1992-2002). Journal of American Veterinary Medical Association 225, 1225-1230.

Liu, Y., Song, Q., Jin, H.T., Lin, X.Z., Chen, K.M., 2009. The value of multidetector-row CT in the preoperative detection of pancreatic insulinomas. La Radiologia Medica 114, 1232-1238.

Madarame, H., Kayanuma, H., Shida, T., Tsuchiya, R., 2009. Retrospective study of canine insulinomas: eight cases (2005-2008). Journal of Veterinary Medical Science 71, 905-911.

Mai, W. and Caceres, A.V., 2008. Dual-phase computed tomographic angiography in three dogs with pancreatic insulinoma. Veterinary Radiology & Ultrasound 49, 141-148.

Martin, R.A., 1993. Congenital portosystemic shunt in the dog and cat. Veterinary Clinics of North America: Small Animal Practice 23, 609-623.

Mehl, M.L., Kyles, A.E., Hardie, M., Kass, P.H., Adin, C.A., Flynn, A.K., De Cock, H.E., Gregory, C.R., 2005. Evaluation of ameroid ring constrictors for treatment for single extrahepatic portosystemic shunts in dogs: 168

cases (1995-2001). Journal of American Veterinary Medical Association 226, 2020-2030.

Nakamura, K., Takagi, S., Sasaki, N., 2010. Contrast-enhanced ultrasonography for characterizeation of canine focal liver lesions. Veterinary Radiology & Ultrasound 51, 79-85.

Nakamura, K., Lim, S.Y., Ochiai, K., Yamasaki, M., Ohta, H., Morishita, K., Takagi, S. and Takiguchi, M. 2014. Contrast-enhanced ultrasonographic findings in three dogs with pancreatic insulinoma. Veterinary Radiology & Ultrasound 56, 55-62.

Nelson, N.C., Nelson, L.L., 2011. Anatomy of extrahepatic portosystemic shunts in dogs as determined by computed tomography angiography. Veterinary Radiology & Ultrasound 52, 498-506.

Nyman, H.T., O'Brien, R.T., 2007. The sonographic evaluation of lymph nodes. Clincal Techniques in Small Animal Practice 22, 128-137.

Patnaik, A.K., Hurvitz, A.I., Lieberman, P.H., 1980. Canine hepatic neoplasms: A clinicopathologic study. Veterinary Pathology 17, 553-564.

Patnaik, A.K., Hurvitz, A.I., Lieberman, P.H., Johnson, G.F., 1981. Canine hepatocellular carcinoma. Veterinary Pathology 18, 427-438.

Patnaik, A.K., Lieberman, P.H., Hurvitz, A.I., Johnson, G.F., 1981. Canine hepatic carcinoid. Veterinary Pathology 18, 445-453.

Penninck, D.G., Zeyen, U., Taeymans, O.N., Webster, C.R., 2013. Ultrasonographic measurement of the pancreas and pancreatic duct in clinically normal dogs. American Journal of Veterinary Research 74, 433-437.

Polton, G. A., White, R. N., Brearley, M. J., Eastwood, J. M., 2007. Improved survival in a retrospective cohort of 28 dogs with insulinoma. Journal of Small Animal Practice 48, 151-156.

Robben, J.H., Pollak, Y.W.E.A., Kirpensteijn, J., Boroffka, S.A.E.B., van den Ingh, T.S.G.A.M., Teske, E., Voorhout, G. 2005. Comparison of ultrasonography, computed tomography, and single-photon emission computed tomography for the detection and localization of canine insulinoma. Journal of Veterinary Internal Medidicne 19, 15-22.

Strombeck, D.R., 1978. Clinicopathologic features of primary and metastatic

neoplastic disease of the liver in dogs. Journal of American Veterinary Medical Association 173, 267-269.

Strombeck, D.R, Guildford, W.G., 1996. Hepatic neoplasms. In: Strombeck DR, Guilford WG. Strombeck's Small Animal Gastroenterology. Third edition. Philadelphia. W.B. Saunders, pp 847-860.

Szatmari, V., Rothuizen. J., 2006. Ultrasonographic identification and characterization of congenital portosystemic shunts and portal hypertensive disorders in dogs and cats. In: WSAVA Liver Standardization Group (Eds). WSAVA Standards for Clinical and Histological Diagnosis of Canine and Feline Liver Diseases. Elsivier, Philadelphia, pp. 15-39.

Taniura, T., Marukawa, K., Yamada, K., Hikasa, Y, Ito, K., 2009. Differential diagnosis of hepatic tumor-like lesions in dog by using dynamic CT scanning. Hiroshima Journal of Medical Science 58, 17-24.

van den Bossche, L., van Steenbeek, F.G., Favier, R.P., Kummeling, A., Leegwater, P.A.J., Rothuizen, J., 2012. Dsitribution fo extrahepatic congenital portosystemic shunt morphology in predisposed dog breeds. BMC Veterinary Research 8, 112.

Vanderperren, K., Haers, H., van der Vekens, E., Stock, E., Paepe, D., Daminet, S. Saunders, J. H. 2013. Description of the use of contrast enhanced ultrasonography in four dogs with pancreatic tumors. Journal of Small Animal Practice 55, 164-169.

Winter, M. D., Kinney, L. M., Kleine, L.J., 2005. Three-dimensional helical computed tomographic angiography of the liver in five dogs. Veterinary Radiology & Ultrasound 46, 494-499.

Zwingenberger, A.L., Schwarz, T., Saunders, M., 2005. Helical computed tomographic angiography of canine portosystemic shunts. Veterinary Radiology & Ultrasound 46, 27-32.